Biological structure and function emerge from scaling unsupervised learning to 250 million protein sequences

Alexander Rives [*1,2] **Joshua Meier** [*1] **Tom Sercu** [*1] **Siddharth Goyal** [*1] **Zeming Lin** [2] **Demi Guo** [3†] **Myle Ott** [1] **C. Lawrence Zitnick** [1] **Jerry Ma** [4†] **Rob Fergus** [2]

Abstract

In the field of artificial intelligence, a combination of scale in data and model capacity enabled by unsupervised learning has led to major advances in representation learning and statistical generation. In the life sciences, the anticipated growth of sequencing promises unprecedented data on natural sequence diversity. Evolutionary-scale language modeling is a logical step toward predictive and generative artificial intelligence for biology. To this end we use unsupervised learning to train a deep contextual language model on 86 billion amino acids across 250 million protein sequences spanning evolutionary diversity. The resulting model contains information about biological properties in its representations. The representations are learned from sequence data alone; no information about the properties of the sequences is given through supervision or domain-specific features. The learned representation space has a multi-scale organization reflecting structure from the level of biochemical properties of amino acids to remote homology of proteins. Information about secondary and tertiary structure is encoded in the representations and can be identified by linear projections. Representation learning produces features that generalize across a range of applications, enabling state-of-the-art supervised prediction of mutational effect and secondary structure, and improving state-of-the-art features for long-range contact prediction.

[*]Equal contribution [†]Work performed while at Facebook AI Research [1]Facebook AI Research [2]Dept. of Computer Science, New York University [3]Harvard University [4]Booth School of Business, University of Chicago & Yale Law School. Correspondence to: Alexander Rives <arives@cs.nyu.edu>. Pre-trained models available at: <https://github.com/facebookresearch/esm>.

1. Introduction

Growth in the number of protein sequences in public databases has followed an exponential trend over decades, creating a deep view into the breadth and diversity of protein sequences across life. This data is a promising ground for studying predictive and generative models for biology using artificial intelligence. Our focus here will be to fit a single model to many diverse sequences from across evolution. Accordingly we study high-capacity neural networks, investigating what can be learned about the biology of proteins from modeling evolutionary data at scale.

The idea that biological function and structure are recorded in the statistics of protein sequences selected through evolution has a long history (Yanofsky et al., 1964; Altschuh et al., 1987; 1988). Out of the possible random perturbations to a sequence, evolution is biased toward selecting those that are consistent with fitness (Göbel et al., 1994). The unobserved variables that determine a protein's fitness, such as structure, function, and stability, leave a record in the distribution of observed natural sequences (Göbel et al., 1994).

Unlocking the information encoded in protein sequence variation is a longstanding problem in biology. An analogous problem in the field of artificial intelligence is natural language understanding, where the distributional hypothesis posits that a word's semantics can be derived from the contexts in which it appears (Harris, 1954).

Recently, techniques based on self-supervision, a form of unsupervised learning in which context within the text is used to predict missing words, have been shown to materialize representations of word meaning that can generalize across natural language tasks (Collobert & Weston, 2008; Dai & Le, 2015; Peters et al., 2018; Devlin et al., 2018). The ability to learn such representations improves significantly with larger training datasets (Baevski et al., 2019; Radford et al., 2019).

Protein sequences result from a process greatly dissimilar to natural language. It is uncertain whether the models and objective functions effective for natural language transfer across differences between the domains. We explore this question by training high-capacity Transformer language

models on evolutionary data. We investigate the resulting unsupervised representations for the presence of biological organizing principles and information about intrinsic biological properties. We find metric structure in the representation space that accords with organizing principles at scales from physicochemical to remote homology. We also find that secondary and tertiary protein structure can be identified in representations. The properties captured by the representations generalize across proteins. We apply the representations to a range of prediction tasks and find that they improve state-of-art features across the applications.

2. Background

Sequence alignment and search is a longstanding basis for comparative and statistical analysis of biological sequence data. (Altschul et al., 1990; Altschul & Koonin, 1998; Eddy, 1998; Remmert et al., 2011). Search across large databases containing evolutionary diversity assembles related sequences into a multiple sequence alignment (MSA). Within sequence families, mutational patterns convey information about functional sites, stability, tertiary contacts, binding, and other properties (Altschuh et al., 1987; 1988; Göbel et al., 1994). Conserved sites correlate with functional and structural importance (Altschuh et al., 1987). Local biochemical and structural contexts are reflected in preferences for distinct classes of amino acids (Levitt, 1978). Covarying mutations have been associated with function, tertiary contacts, and binding (Göbel et al., 1994).

The prospect of inferring biological structure and function from evolutionary statistics has motivated development of machine learning on individual sequence families. Covariance, correlation, and mutual information have confounding effects from indirect couplings (Weigt et al., 2009). Maximum entropy methods disentangle direct interactions from indirect interactions by inferring parameters of a posited generating distribution for the sequence family (Weigt et al., 2009; Marks et al., 2011; Morcos et al., 2011; Jones et al., 2011; Balakrishnan et al., 2011; Ekeberg et al., 2013b). The generative picture can be extended to include latent variables (Riesselman et al., 2018).

Recently, self-supervision has emerged as a core direction in artificial intelligence research. Unlike supervised learning which requires manual annotation of each datapoint, self-supervised methods use unlabeled datasets and thus can exploit far larger amounts of data. Self-supervised learning uses proxy tasks for training, such as predicting the next word in a sentence given all previous words (Bengio et al., 2003; Dai & Le, 2015; Peters et al., 2018; Radford et al., 2018; 2019) or predicting words that have been masked from their context (Devlin et al., 2018; Mikolov et al., 2013).

Increasing the dataset size and the model capacity has shown improvements in the learned representations. In recent work, self-supervision methods used in conjunction with large data and high-capacity models produced new state-of-the-art results approaching human performance on various question answering and semantic reasoning benchmarks (Devlin et al., 2018), and coherent natural text generation (Radford et al., 2019).

This paper explores self-supervised language modeling approaches that have demonstrated state-of-the-art performance on a range of natural language processing tasks, applying them to protein data in the form of unlabeled amino acid sequences. Since protein sequences use a small vocabulary of twenty canonical elements, the modeling problem is more similar to character-level language models (Mikolov et al., 2012; Kim et al., 2016) than word-level models. Like natural language, protein sequences also contain long-range dependencies, motivating use of architectures that detect and model distant context (Vaswani et al., 2017).

3. Scaling language models to 250 million diverse protein sequences

Large protein sequence databases contain diverse sequences sampled across life. In our experiments we explore datasets with up to 250 million sequences of the Uniparc database (The UniProt Consortium, 2007) which has 86 billion amino acids. This data is comparable in size to large text datasets that are being used to train high-capacity neural network architectures on natural language (Devlin et al., 2018; Radford et al., 2019). To model the data of evolution with fidelity, neural network architectures must have capacity and inductive biases to represent its breadth and diversity.

We investigate the Transformer (Vaswani et al., 2017), which has emerged as a powerful general-purpose model architecture for representation learning and generative modeling, outperforming recurrent and convolutional architectures in natural language settings. We use a deep Transformer (Devlin et al., 2018) with character sequences of amino acids from the proteins as input.

The Transformer processes inputs through a series of blocks that alternate self-attention with feed-forward connections. Self-attention allows the network to build up complex representations that incorporate context from across the sequence. Since self-attention explicitly constructs pairwise interactions between all positions in the sequence, the Transformer architecture directly represents residue-residue interactions.

We train models using the masked language modeling objective (Devlin et al., 2018). Each input sequence is corrupted by replacing a fraction of the amino acids with a special mask token. The network is trained to predict the missing tokens from the corrupted sequence:

	Model		Params	Training	ECE
(a)	Oracle				1
	Uniform Random				25
(b)	n-gram	4-gram		UR50/S	17.18
(c)	LSTM biLM	Small	28.4M	UR50/S	14.42
	LSTM biLM	Large	113.4M	UR50/S	13.54
(d)	Transformer	6-layer	42.6M	UR50/S	11.79
	Transformer	12-layer	85.1M	UR50/S	10.45
(e)	Transformer	34-layer	669.2M	UR100	10.32
	Transformer	34-layer	669.2M	UR50/S	8.54
	Transformer	34-layer	669.2M	UR50/D	**8.46**
(f)	Transformer	10% data	669.2M	UR50/S	10.99
	Transformer	1% data	669.2M	UR50/S	15.01
	Transformer	0.1% data	669.2M	UR50/S	17.50

Table 1. Evaluation of language models for generalization to held-out UniRef50 clusters. (a) Exponentiated cross-entropy (ECE) ranges from 25 for a random model to 1 for a perfect model. (b) Best n-gram model across range of context sizes and Laplace-smoothing settings. (c) State-of-the-art LSTM bidirectional language models (Peters et al., 2018). (d) Transformer model baselines with 6 and 12 layers. Small Transformer models have better performance than LSTMs despite having fewer parameters. (e) 34-layer Transformer models trained on datasets of differing sequence diversity. Increasing the diversity of the training set improves generalization. High-capacity Transformer models outperform LSTMs and smaller Transformers. (f) 34-layer Transformer models trained on reduced fractions of data. Increasing training data improves generalization.

$$\mathcal{L}_{\text{MLM}} = \mathbb{E}_{x\sim X}\ \mathbb{E}_{M}\ \sum_{i\in M} -\log p(x_i|x_{/M}) \qquad (1)$$

For each sequence x we sample a set of indices M to mask, replacing the true token at each index i with the mask token. For each masked token, we independently minimize the negative log likelihood of the true amino acid x_i given the masked sequence $x_{/M}$ as context. Intuitively, to make a prediction for a masked position, the model must identify dependencies between the masked site and the unmasked parts of the sequence.

Evaluation of language models We begin by training a series of Transformers on all the sequences in UniParc (The UniProt Consortium, 2007), holding out a random sample of 1M sequences for validation. We use these models throughout to investigate properties of the representations and the information learned during pre-training.

To comparatively evaluate generalization performance of different language models we use UniRef50 (Suzek et al., 2015), a clustering of UniParc at 50% sequence identity. For evaluation, a held-out set of 10% of the UniRef50 clusters is randomly sampled. The evaluation dataset consists of the representative sequences of these clusters. All sequences belonging to the held-out clusters are removed from the pre-training datasets for subsequent experiments.

We explore the effect of the underlying sequence diversity in the pre-training data. Clustering UniParc shows a power-law distribution of cluster sizes (Suzek et al., 2007), implying the majority of sequences belong to a small fraction of clusters. We use UniRef (Suzek et al., 2015) to create three pre-training datasets with differing levels of diversity: (i) the low-diversity dataset (UR100) uses the UniRef100 representative sequences; (ii) the high-diversity sparse dataset (UR50/S) uses the UniRef50 representative sequences; (iii) the high-diversity dense dataset (UR50/D) samples the UniRef100 sequences evenly across the UniRef50 clusters.

Table 1 presents modeling performance on the held-out UniRef50 sequences across a series of experiments exploring different model classes, number of parameters, and pre-training datasets. Models are compared using the exponentiated cross entropy (ECE) metric, which is the exponential of the model's loss averaged per token. In the case of the Transformer this is $2^{\mathcal{L}_{\text{MLM}}}$. ECE describes the mean uncertainty of the model among its set of options for every prediction: ranging from 1 for an ideal model to 25 (the number of unique amino acid tokens in the data) for a completely random prediction. To quantify the difficulty of generalization to the evaluation set, we train a series of n-gram models across a range of context lengths and settings of Laplace smoothing on UR50/S. The best n-gram model has an ECE of 17.18 with context size of 4.

As a baseline we train recurrent LSTM bidirectional language models (Peters et al., 2018), which are state-of-the-art for recurrent models in the text domain: a small model with approximately 25M parameters, and a large model with approximately 113M parameters. Trained on the UR50/S

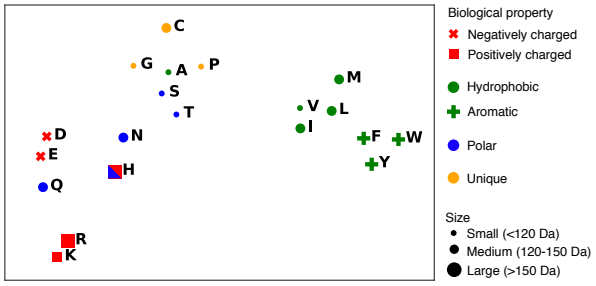

Figure 1. Biochemical properties of amino acids are represented in the Transformer model's output embeddings, visualized here with t-SNE. Through unsupervised learning, residues are clustered into hydrophobic, polar, and aromatic groups, and reflect overall organization by molecular weight and charge. Visualization of 36-layer Transformer trained on UniParc.

dataset, the small and large LSTM models have an ECE of 14.4 and 13.5 respectively.

We also train two small Transformers, a 12-layer (85.1M parameters) and 6-layer Transformer (42.6M parameters) on the UR50/S dataset. Both Transformer models have better ECE values (10.45, and 11.79 respectively) than the small and large LSTM models, despite the large LSTM having more parameters. These results show the Transformer enables higher fidelity modeling of protein sequences for a comparable number of parameters.

We train high-capacity 34-layer Transformers (approx 670M parameters) across the three datasets of differing diversity. The high-capacity Transformer model trained on the UR50/S dataset outperforms the smaller Transformers indicating an improvement in language modeling with increasing model capacity. Transformers trained on the two high-diversity datasets, UR50/S and UR50/D, improve generalization over the UR100 low-diversity dataset. The best Transformer trained on the most diverse and dense dataset reaches an ECE of 8.46, corresponding intuitively to the model choosing among approximately 8.46 amino acids for each prediction.

We also train a series of 34-layer Transformer models on 0.1%, 1%, and 10% of the UR50/S dataset, seeing the expected relationship between increased data and improved generalization performance. Underfitting is observed even for the largest models trained on 100% of UR50/S suggesting potential for additional improvements with higher capacity models.

4. Multi-scale organization in sequence representations

The variation observed in large protein sequence datasets is influenced by processes at many scales, including properties that affect fitness directly, such as activity, stability, structure, binding, and other properties under selection (Hormoz, 2013; Hopf et al., 2017) as well as by contributions from phylogenetic bias (Gabaldon, 2007), experimental and selection biases (Wang et al., 2019; Overbaugh & Bangham, 2001), and sources of noise such as random genetic drift (Kondrashov et al., 2003).

Unsupervised learning may encode underlying factors that, while unobserved, are useful for explaining the variation in sequences seen by the model during pre-training. We investigate the representation space of the network at multiple scales from biochemical to evolutionary homology to look for signatures of biological organization.

Neural networks contain inductive biases that impart structure to representations. Randomly initialized networks can produce features that perform remarkably well without any learning (Jarrett et al., 2009). To understand how the process of learning shapes the representations, it is necessary to compare representations before and after they have been trained. Furthermore, a basic level of intrinsic organization is expected in the sequence data itself as a result of biases in amino acid composition. To disentangle the role of frequency bias in the data we also compare against a baseline that maps each sequence to a vector of normalized amino acid counts.

Learning encodes biochemical properties The Transformer neural network represents the identity of each amino acid in its input and output embeddings. The input embeddings project the input amino acid tokens into the first Transformer block. The output embeddings project the final hidden representations back to logarithmic probabilities. The interchangeability of amino acids within a given structural/functional context in a protein depends on their biochemical properties (Hormoz, 2013). Self-supervision can be expected to capture these patterns to build a representation space that reflects biochemical knowledge.

To investigate if the network has learned to encode physicochemical properties in representations, we project the weight matrix of the final embedding layer of the network into two dimensions with t-SNE (Maaten & Hinton, 2008). In Figure 1 the structure of the embedding space reflects biochemical interchangeability with distinct clustering of hydrophobic and polar residues, aromatic amino acids, and organization by molecular weight and charge.

Biological variations are encoded in representation space Each protein can be represented as a single vec-

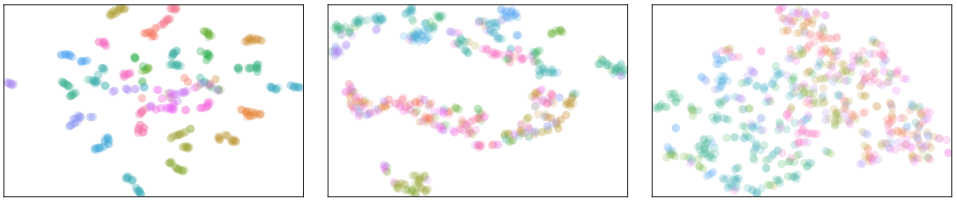

Transformer (trained) Transformer (untrained) Unigram

(a) Sequence representations (t-SNE)

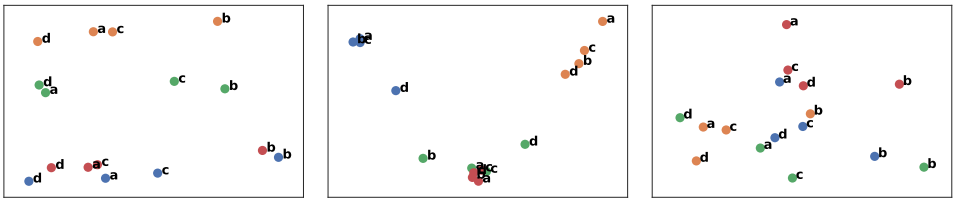

Transformer (trained) Transformer (untrained) Unigram

(b) Sequence representations (PCA)

Figure 2. Protein sequence representations encode and organize biological variations. (a) Each point represents a gene, and each gene is colored by the orthologous group it belongs to (dimensionality is reduced by t-SNE). Orthologous groups of genes are densely clustered in the trained representation space. By contrast, the untrained representation space and unigram representations do not reflect strong organization by evolutionary relationships. (b) Genes corresponding to a common biological variation are related linearly in the trained representation space. Genes are colored by their orthologous group, and their species is indicated by a character label. PCA recovers a species axis (horizontal) and orthology axis (vertical) in the trained representation space, but not in the untrained or unigram spaces. Representations are from the 36-layer Transformer model trained on UniParc.

tor by averaging across the final hidden representation at each position in its sequence. Protein embeddings represent sequences as points in high dimensional space. Each sequence is represented as a single point and sequences assigned to similar representations by the network are mapped to nearby points. We investigate how homologous genes are represented in this space.

The structure and function of orthologous genes is likely to be retained despite divergence of their sequences (Huerta-Cepas et al., 2018). We find in Figure 2a that training shapes the representation space so that orthologous genes are clustered. Figure 2a shows a two-dimensional projection of the model's representation space using t-SNE. Prior to training the organization of orthologous proteins in the model's representation space is diffuse. Orthologous genes are clustered in the learned representation space.

We examine whether unsupervised learning encodes biological variations into the structure of the representation space. We apply principal component analysis (PCA), to recover principal directions of variation in the representations, selecting 4 orthologous genes across 4 species to look for directions of variation. Figure 2b indicates that linear dimensionality reduction recovers species and orthology as primary axes of variation in the representation space after training. This form of structure is absent from the representations prior to training.

To quantitatively investigate the structure of the representation space, we assess nearest neighbor recovery under vector similarity queries. If biological properties are encoded along independent directions in the representation space, then proteins corresponding with a unique biological variation are related by linear vector arithmetic. In Figure S1 we find that learning improves recovery of target proteins under queries encoded as linear transformations along the species or gene axes.

Learning encodes remote homology Remotely homologous proteins have underlying structural similarity despite divergence of their sequences. If structural homology is encoded in the metric structure of the representation space, then the distance between proteins in the representation space reflects their degree of structural relatedness.

We investigate whether the representation space enables detection of remote homology at the superfamily (proteins that belong to different families but are in the same superfamily) and fold (proteins that belong to different superfamilies but have the same fold) level. We construct a dataset of remote homolog pairs derived from SCOP (Fox et al., 2013), following standard practices to exclude folds that are known to be related (Dunbrack Jr, 2006).

	Pre-training	Hit-10 Fold	Hit-10 SF	AUC Fold	AUC SF
HHblits†		.584	.965	.831	.951
LSTM(S)	UR50/S	.558	.760	.801	.863
LSTM(L)	UR50/S	.574	.813	.805	.880
Transf-6	UR50/S	**.653**	.878	.768	.901
Transf-12	UR50/S	.639	.915	.778	**.942**
Transf-34	None	.481	.527	.755	.807
Transf-34	UR100	.599	.841	.753	.876
Transf-34	UR50/D	.617	**.932**	.822	.932
Transf-34	UR50/S	.639	.931	**.825**	.933

Table 2. Remote homology at the fold and superfamily (SF) level is encoded in the metric structure of the representation space. Results for unsupervised classifier based on distance between vector sequence embeddings. Hit-10 reports the probability that a remote homolog is included in the ten nearest neighbors of the query sequence. Area under the ROC curve (AUC) is reported for classification by distance from the query in representation space. Transformer models have higher performance than LSTMs and similar performance to HMMs at the fold level. Best neural models are indicated in bold. † HHblits (Remmert et al., 2011), a state-of-the-art HMM-based method for remote homology detection, using 3 iterations of sequence search.

For each domain, a vector similarity query is performed against all other domains, ranking them by distance to the query domain. An unsupervised classifier on distance from the query measures the density of homologous proteins in the neighborhood of a query. We report AUC for the classifier, and Hit-10 which gives the probability of recovering a remote homolog in the ten highest ranked results, and has been used in the literature on remote homology detection (Ma et al., 2014).

Table 2 indicates that vector nearest neighbor queries using the representations can detect remote homologs that are distant at the fold level with similar performance to HHblits (Remmert et al., 2011) a state-of-the-art HMM-HMM alignment-based method. At the superfamily level, where sequence similarity is higher, HMM performance is better, but Transformer-based embeddings are close. Fast vector nearest neighbor finding methods allow billions of sequences to be searched for similarity to a query protein within milliseconds (Johnson et al., 2017).

Learning encodes information in multiple sequence alignments An MSA identifies corresponding sites across a family of related sequences (Ekeberg et al., 2013a). These correspondences give a picture of evolutionary variation at different sites within the sequence family. The model receives as input individual sequences and is given no access to the family of related sequences except via learning.

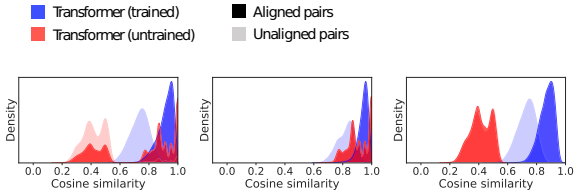

(a) Overall (b) Identical A.A. pairs (c) Distinct A.A. pairs

Figure 3. Final representations from trained models implicitly align sequences. Cosine similarity distributions are depicted for the final representations of residues from sequences within PFAM family PF01010. The differences between the aligned (dark blue) and unaligned (light blue) distributions imply that the trained Transformer representations are a powerful discriminator between aligned and unaligned positions in the sequences. In contrast representations prior to training do not separate the aligned (dark red) and unaligned positions (light red). AUCs across 128 PFAM families are reported in Table S3.

We investigate whether the final hidden representations of a sequence encode information about the family it belongs to.

Family information could appear in the network through assignment of similar representations to positions in different sequences that are aligned in the family's MSA. Using the collection of MSAs of structurally related sequences in Pfam (Bateman et al., 2013), we compare the distribution of cosine similarities of representations between pairs of residues that are aligned in the family's MSA to a background distribution of cosine similarities between unaligned pairs of residues. A large difference between the aligned and unaligned distributions implies that the representations use shared features for related sites within all the sequences of the family.

Figure 3a depicts the distribution of cosine similarity values between aligned and unaligned positions within a representative family for the trained model and baselines. Unsupervised learning produces a marked shift between the distributions of aligned and unaligned pairs. Figure 3b and Figure 3c indicate that these trends hold under the constraints that the residue pairs (1) share the same amino acid identity or (2) have different amino acid identities.

We estimate differences between the aligned and unaligned distributions across 128 Pfam families using the area under the ROC curve (AUC) as a metric of discriminative power between aligned and unaligned pairs. Table S3 shows a quantitative improvement in average AUC after unsupervised training, supporting the idea that self-supervision encodes information about the MSA of a sequence into its representation of the sequence.

5. Prediction of secondary structure and tertiary contacts

Through unsupervised pre-training with a language modeling objective, the Transformer learns to map each protein into a sequence of high-dimensional latent representations. In the previous section we find that the structure of this representation space encodes relational properties of proteins at different scales. We now explore if the representations also capture intrinsic structural properties of proteins.

There is reason to believe that unsupervised learning will cause the model's representations to contain structural information. The underlying structure of a protein is a hidden variable that influences the patterns observed in sequence data. For example local sequence variation depends on secondary structure (Levitt, 1978); and tertiary structure introduces higher order dependencies in the choices of amino acids at different sites within a protein (Marks et al., 2011; Anishchenko et al., 2017). While the model cannot observe protein structure directly, it observes patterns in the sequences of its training data that are determined by structure. In principle, the network could compress sequence variations by capturing commonality in structural elements across the data, thereby encoding structural information into the representations.

We begin by identifying information about protein structure that is linearly encoded within the representations. The use of linear projections ensures that the information originates in the Transformer representations, enabling a direct inspection of the structural content of representations. By comparing representations of the Transformer before and after pre-training, we can identify the information that emerges as a result of the unsupervised learning.

We then train deep neural networks to predict secondary and tertiary structure from the representations. We choose architectures which are state-of-the-art for secondary structure prediction and residue-residue contact prediction. These downstream models are trained with a supervised loss to predict either the secondary structure or contact map from the pre-trained representations. The architecture of the downstream model is kept fixed across experiments with different representations and baselines to enable comparison. The models are evaluated against a panel of test sets, using sequence identity-based hold-out or temporal hold-out for the evaluation sets.

5.1. Secondary structure

Linear projection To identify information about secondary structure a linear projection is fit mapping the pre-trained representation at each position to the eight-class secondary structure assignment. Projections are fit via multi-class logistic regression to a training set (Zhou & Troyanskaya, 2014) which implements a 25% sequence identity hold-out with the CB513 benchmark (Cuff & Barton, 1999).

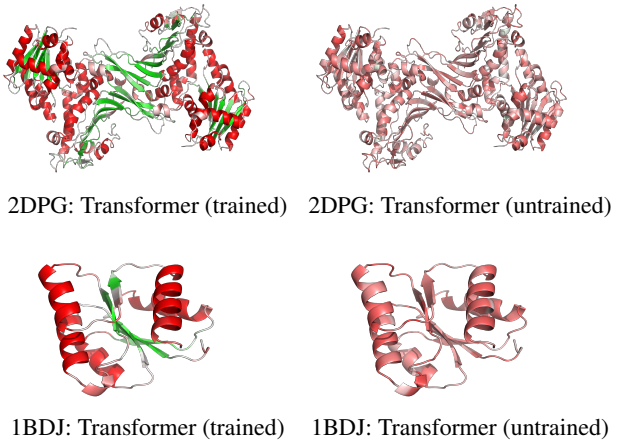

Figure 4. Linear projections of final hidden representations (36-layer UniParc Transformer). Unsupervised pre-training encodes secondary structure into representations. Following pre-training, linear projections recover secondary structure (left column). Without pre-training little information is recovered (right column). Colors indicate secondary structure class identified by the projection: helix (red), strand (green), and coil (white). Color intensities indicate confidence. Here 3-class linear projections are visualized for two test proteins 2DPG (Cosgrove et al., 1998) and 1BDJ (Kato et al., 1999). Linearly recoverable information across the CB513 test set is reported in Table S4.

The neural representations are compared to (i) an amino-acid prior that predicts the most likely label for each amino acid, and (ii) a position-specific scoring matrix (PSSM) for each protein. Without pre-training, as visualized in Figure 4, minimal information about secondary structure can be identified. After pre-training, linear projections recover information in the model representations above the amino-acid prior and PSSM features. Figure S2 shows that a rapid increase in the linearly encoded information about secondary structure occurs in the initial stages of training. Accuracy across the CB513 evaluation set is reported in Table S4.

Deep neural network We replace the linear layer with a deep neural network, using the hybrid convolutional/recurrent model architecture introduced by the Netsurf method (Klausen et al., 2019). The Netsurf model (and other state-of-the-art neural methods for secondary structure prediction) use sequence profiles, requiring an MSA for each input protein. Here we replace these features with the automatically learned representations of the Transformer model. We evaluate models on the CB513 test set and the CASP13 domains (Kryshtafovych et al., 2019). For comparison we also re-implement the Netsurf method and features. Models are trained on the Netsurf training dataset which applies a 25% sequence identity hold-out with CB513, and

Model	Pre-Training	CB513	CASP13
Transf-34	None	56.8 ± 0.3	60.0 ± 0.5
LSTM(S)	UR50/S	60.4 ± 0.1	63.2 ± 0.6
LSTM(L)	UR50/S	62.4 ± 0.2	64.1 ± 0.7
Transf-6	UR50/S	62.0 ± 0.2	64.2 ± 1.2
Transf-12	UR50/S	65.4 ± 0.1	67.2 ± 0.3
Transf-34	UR100	64.3 ± 0.2	66.5 ± 0.3
Transf-34	UR50/S	$\mathbf{69.1 \pm 0.2}$	$\mathbf{70.7 \pm 0.8}$
Transf-34	UR50/D	$\mathbf{69.2 \pm 0.1}$	$\mathbf{70.9 \pm 0.5}$

Table 3. Eight-class secondary structure prediction accuracy on the CB513 and CASP13 test sets. A fixed neural architecture is trained to predict the secondary structure label from the language model representation of the input sequence. The Transformer has higher performance than the comparable LSTM baselines. Pre-training with the two high-diversity datasets (UR50/S and UR50/D) increases accuracy significantly.

a temporal hold-out with CASP13.

Table 3 compares the representations for secondary structure prediction. The Transformer features are compared before and after unsupervised pre-training to features from the LSTM baselines. The best Transformer features (69.2%) are close in performance to our re-implementation of Netsurf (71.2%) and the published performance of RaptorX (70.6)% on the same benchmark (Klausen et al., 2019). The Transformer representations produce higher accuracy than the LSTM baselines with comparable numbers of parameters.

Table 3 also evaluates the effect of sequence diversity on downstream performance. The diversity of the sequence data used in pre-training strongly influences the quality of the features: pre-training with the two high-diversity datasets (UR50/S and UR50/D) produces a significant improvement in accuracy over features from the low-diversity dataset (UR100).

Relationship between language modeling and secondary structure prediction To investigate the relationship between pre-training ECE and performance on the downstream task, the downstream model is trained on features from Transformer models taken from across their pre-training trajectories. We use the pre-training checkpoints for the Transformers trained on UR50/S. Averages are computed across three independent seeds of the downstream model per Transformer checkpoint. For each model, Figure 5 shows a linear relationship between ECE and secondary structure prediction accuracy, which holds over the course of pre-training. The linear fit is close to ideal; for example, the 34-layer model has $R^2 = .99$. Thus, for a given model and pre-training dataset, language modeling fidelity measured by ECE is a good proxy for the structural content of the representations. Since ECE improves with model capacity, this suggests further scale may increase performance on structure prediction tasks.

Representation	PF00005	PF00069	PF00072
Amino acid identity	0.516	0.506	0.536
12-layer (untrained)	0.818	0.719	0.835
12-layer (PF00005)	<u>0.864</u>	0.725	0.842
12-layer (PF00069)	0.816	<u>0.842</u>	0.850
12-layer (PF00072)	0.789	0.688	<u>0.888</u>
12-layer (UniParc)	0.900	0.872	**0.906**
36-layer (UniParc)	**0.902**	**0.884**	0.902

Table 4. Three-class secondary structure prediction accuracy by linear projection. Learning across many protein families produces better representations than learning from single protein families. Transformer models are trained on three PFAM families: ATP-binding domain of the ABC transporters (PF00005), Protein kinase domain (PF00069), and Response regulator receiver domain (PF00072). The single-family models are contrasted with models trained on the full UniParc data. Comparisons are relative to the family (columnwise), since each of the families differ in difficulty. Underline indicates models trained and evaluated on the same family. Representations learned from single families perform well within the family, but do not generalize as well to sequences outside the family. Representations trained on UniParc outperform the single-family representations in all cases.

Single versus multi-family pre-training We compare training across evolutionary statistics to training on single protein families. We pre-train separate 12-layer Transformer models on the Pfam multiple sequence alignments of the three most common domains in nature longer than 100 amino acids, the ATP-binding domain of the ABC transporters, the protein kinase domain, and the response regulator receiver domain. We test the ability of models trained on one protein family to generalize secondary structure information within-family and out-of-family by evaluating on sequences with ground truth labels from the family the model was trained on or from the alternate families. The models are evaluated using linear projections. In all cases, the model trained on within-family sequences has higher accuracy than models trained on out-of-family sequences (Table 4), indicating poor generalization when training on single MSA families. More significantly, the model trained across the full UniParc sequence diversity has a higher accuracy than the single-family model accuracies, even on the same-family evaluation dataset. This suggests that the representations learned from the full dataset are generalizing information about secondary structure learned outside the sequence family.

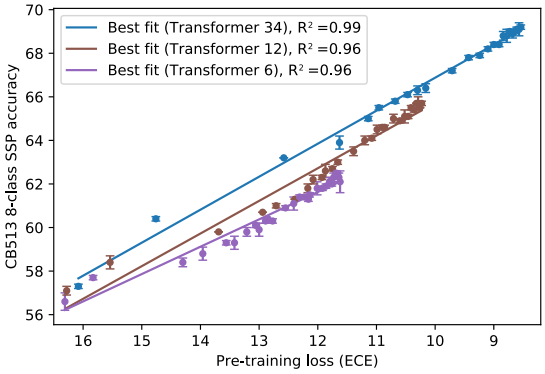

Figure 5. Eight-class secondary structure prediction accuracy as a function of pre-training ECE. A deep secondary structure predictor is trained using features from Transformer models over the course of pre-training on UR50/S. Averages across three seeds of the downstream model per pre-training checkpoint are plotted, with line of best fit for each Transformer. The linear relationship for each model indicates that for a given model and pre-training dataset, language modeling ECE is a good proxy for performance on the downstream task. This establishes a link between language modeling performance and structure prediction, suggesting that increasing model size further may lead to improvements in results.

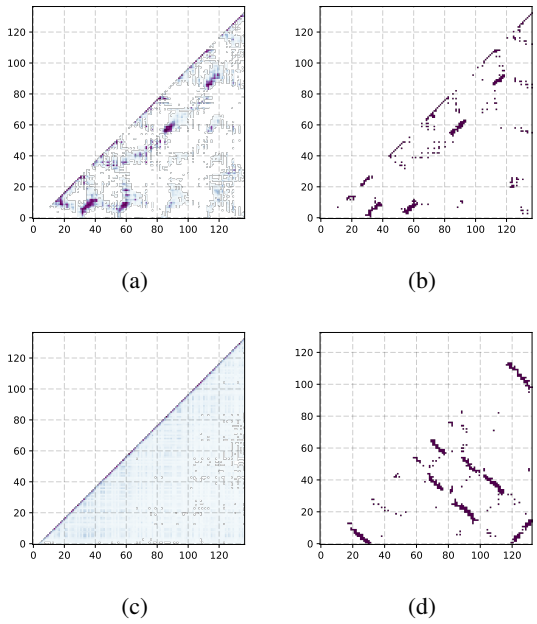

Figure 6. Linear projections of final hidden representations (36-layer UniParc Transformer) visualized as pairwise contact maps. Unsupervised pre-training discovers information about tertiary structure. After pre-training, linear projections from the final layer representations (a) recover a contact pattern similar to the ground truth (b). Without pre-training, no meaningful predictions can be made (c). The different contact pattern of the nearest neighbor in the training data by sequence identity (d) indicates that the model is not simply transferring information via sequence similarity. Visualization is shown for B12-binding subunit of glutamate mutase from *Clostridium cochlearium* (PDB: 1B1A; Hoffmann et al., 1999). Additional visual examples are given in Figure S6. Average AUCs for linear recovery of contacts across the CATH test set are reported in Table S5.

5.2. Residue-residue contacts

Linear projections To identify information about tertiary structure, we fit linear projections to the final hidden representations of pairs of positions in the protein, regressing a binary variable indicating whether the positions are in contact in the protein's 3-dimensional structure. Training and test sets are derived from CATH S40 (Orengo et al., 1997), applying a 20% sequence identity hold-out.

Figure 6 shows an example of contacts recovered by the linear projections of the final hidden representations for a domain in the test set. Before pre-training, no contact patterns can be recovered. After pre-training, projections recover complex contact patterns, including long range contacts. The nearest neighbor by sequence identity in the training data shows a completely different contact map from the ground-truth structure, indicating generalization beyond sequence similarity. Additional examples for domains in the test set having diverse folds are shown in Figure S6. Average AUCs for linear recovery of contacts are given in Table S5.

Deep neural network We train a deep neural network to predict the binary contact map of a protein from its sequence representation. The architecture is a dilated convolutional residual network similar to recent state-of-the-art methods for tertiary structure prediction (Xu, 2018; Jones & Kandathil, 2018; Senior et al., 2018).

Features from different language models are compared across a panel of four test sets using this fixed architecture and the RaptorX training set introduced by Wang et al. (2017). The Test (Wang et al., 2017) and CASP11 (Moult et al., 2016) test sets evaluate with sequence identity hold-out at 25%; the CASP12 (Moult et al., 2018) test set implements a temporal hold-out with the structural training data; and the CASP13 (Kryshtafovych et al., 2019) experiment implements a full temporal hold-out of both the pre-training and training data.

Table 5 shows performance of the various representations for predicting long range contacts across a panel of benchmarks. Top-L precision is the precision of the L (length of the protein) highest ranked predictions by the model for contacts with sequence separation of at least 24 residues. For comparison we train the same architecture using features from RaptorX (Wang et al., 2017; Xu, 2018). For contact prediction, the best features from representation learning do

Model	Pre-training	Test	CASP 11	CASP 12	CASP 13
Transf-34	(None)	16.3	17.7	14.8	13.3
LSTM(S)	UR50/S	24.1	23.6	19.9	15.3
LSTM(L)	UR50/S	27.8	26.4	24.0	16.4
Transf-6	UR50/S	30.2	29.9	25.3	19.8
Transf-12	UR50/S	37.7	33.6	27.8	20.7
Transf-34	UR100	32.7	28.9	24.3	19.1
Transf-34	UR50/S	**50.2**	42.8	**34.7**	**30.1**
Transf-34	UR50/D	50.0	**43.0**	33.6	28.0

Table 5. Top-L long-range contact precision. A deep dilated convolutional residual network is trained to predict contacts using the representations from the pre-trained language model. The pre-trained Transformer representations outperform the LSTM representations in all cases. Pre-training on the high-diversity datasets (UR50/S and UR50/D) boosts precision of representations over pre-training on UR100. High-capacity Transformers (34 layer) outperform lower capacity models (6/12 layer).

Features	CB513	CASP13
RaptorX	70.6	
Netsurf	72.1	74
(a) Netsurf (reimpl.)	71.2 ± 0.1	72.3 ± 0.9
(b) +direct	72.1 ± 0.1	72.2 ± 0.5
(c) +avg	$\mathbf{73.7} \pm \mathbf{0.2}$	$\mathbf{75.1} \pm \mathbf{0.4}$

Table 6. Combining Transformer and state-of-the-art features for secondary structure prediction (eight-class accuracy). Features from a reimplementation of Netsurf (Klausen et al., 2019) are combined with 34-layer Transformer (UR50/S) embeddings using a two layer BiLSTM architecture. (a) Performance of Netsurf features alone. (b) *Direct* adds the Transformer representation of the input sequence. (c) *Avg* adds the average of Transformer features for each position in the MSA of the input sequence. Results exceed those reported for state-of-the-art methods RaptorX (70.6%) and Netsurf (72.1%) on the CB513 test set, and for Netsurf (74.0%) on the CASP13 evaluation set used here. Thus representation learning improves state-of-the-art features for secondary structure prediction.

not achieve comparable performance to the state-of-the-art RaptorX features (50.2 vs 59.4 respectively on the RaptorX test set). Transformer representations yield higher precision than LSTMs, with even the smallest Transformer representations exceeding LSTMs with more parameters. Diversity in the pre-training data also has a strong effect, with the high-diversity datasets providing significant improvements over the low-diversity dataset. Relative performance of the representations is consistent across all four of the benchmarks using different hold-out methodology.

6. Representation learning improves state-of-the-art features for structure prediction

We now explore how features discovered by unsupervised learning can be combined with state-of-the-art features to improve them further. Current state-of-the-art methods use information derived from MSAs. Here we combine this information with features from the Transformer model.

We explore three approaches for incorporating information from representation learning. For each input sequence s: (i) *direct* uses the final hidden representation from the Transformer directly; (ii) *avg* takes the average of the final hidden representation at each position across the sequences from the MSA of s; (iii) *cov* produces features for each pair of positions, using the uncentered covariance across sequences from the MSA of s, after dimensionality reduction of the final hidden representations by PCA. Note that (i) and (ii) produce features for each position in s, while (iii) produces features for each pair of positions.

Secondary structure Current state-of-the-art methods for secondary structure prediction have high accuracies for the eight-class prediction problem (Q8). For example on the widely used CB513 test set, Netsurf (Klausen et al., 2019) reports an accuracy of 72.1%. RaptorX (Wang et al., 2016), another state-of-the-art method has an accuracy of 70.6% on the same benchmark (Klausen et al., 2019).

We investigate whether performance can be improved by combining Transformer features with evolutionary profiles. Table 6 shows that combining the representations with profiles further boosts accuracy, resulting in state-of-the-art performance on secondary structure prediction.

We establish a baseline of performance by replicating the Klausen et al. (2019) architecture and features, achieving an accuracy of 71.2% on the CB513 test set. Then we add the the Transformer features using the direct and avg combination methods; these achieve 0.9% and 2.5% absolute improvement in accuracy respectively. This suggests that the Transformer features contain information not present in the MSA-derived features.

Residue-residue contacts Deep neural networks have enabled recent breakthroughs in the prediction of protein contacts and tertiary structure (Xu, 2018; Senior et al., 2018). State-of-the-art neural networks for tertiary structure and contact prediction use deep residual architectures with two-dimensional convolutions over pairwise feature maps to output a contact prediction or distance potential for each pair of residues (Wang et al., 2017; Xu, 2018; Senior et al., 2018).

	Test	CASP11	CASP12	CASP13
# domains	500	105	55	34
(a) RaptorX	59.4 ± .2	53.8 ± .3	51.1 ± .2	43.4 ± .4
(b) +direct	61.7 ± .4	55.0 ± .1	51.5 ± .5	43.7 ± .4
(c) +avg	62.9 ± .4	56.6 ± .4	52.4 ± .5	44.8 ± .8
(d) +cov	**63.3 ± .2**	**56.8 ± .2**	**53.0 ± .3**	**45.2 ± .5**

Table 7. Top-L long-range contact precision. Combining Transformer and state-of-the-art features for contact prediction. A deep ResNet with fixed architecture is trained on each feature set to predict binary contacts. (a) performance of state-of-the-art RaptorX (Xu, 2018) features including PSSM, predicted secondary structure, predicted accessibility, pairwise APC-corrected Potts model couplings and mutual information, and a pairwise contact potential. (b) Adds Transformer representation of the input sequence to the feature set. (c) Adds the average Transformer representation at each position of the MSA. (d) Adds the uncentered covariance over the MSA of a low-dimenensional projection of the Transformer features. Features are from the 34-layer Transformer pre-trained on UR50/S. Note that the comparison is relative across the features, with absolute numbers for the RaptorX features below their performance in CASP13 due to the use of a different training set of 6,767 proteins from Wang et al. (2017), used across all test sets. The pre-trained features consistently improve performance of the RaptorX features across test sets.

A variety of input features, training datasets, and supervision signals are used in state-of-the-art methods for contact prediction. To make a controlled comparison, we fix a standard architecture, training dataset, multiple sequence alignments, and set of base input features for all experiments, to which we add pre-trained features from the Transformer model. For the base features we use the RaptorX feature set which includes PSSM, 3-state secondary structure prediction, one-hot embedding of sequence, APC corrected Potts model couplings, mutual information, pairwise contact potential, and predicted accessibility. RaptorX was the winning method for contact prediction in the CASP12 and CASP13 competitions (Xu, 2018). The training and evaluation sets are the same as used in the previous section.

Table 7 indicates that addition of Transformer features from the 34-layer model trained on UR50/S consistently produces an improvement across the test sets. The table shows precision on long range (LR) for top-L thresholds reporting mean and standard deviation over 5 different model seeds. *Direct* gives a modest improvement on some test sets. *Avg* improves over direct, and *cov* provides further gains. For example, *cov* produces an absolute improvement of 3.9% on the RaptorX Wang et al. (2017) test set, and 1.8% improvement on the CASP13 test set evaluated with temporal hold-outs on both fine-tuning and pre-training data. Additional results and metrics for contact prediction are reported in Table S6.

7. Representation learning is comparable to state-of-the-art features for predicting mutational effects

The mutational fitness landscape provides deep insight into biology: determining protein activity (Fowler & Fields, 2014), linking genetic variation to human health (Lek et al., 2016; Bycroft et al., 2018; Karczewski et al., 2019), and informing rational protein engineering (Slaymaker et al., 2016). Computational variant effect predictors are useful for assessing the effect of point mutations (Gray et al., 2018; Adzhubei et al., 2013; Kumar et al., 2009; Hecht et al., 2015; Rentzsch et al., 2018). Often their predictions are based on basic evolutionary, physicochemical, and protein structural features that have been selected for their relevance to protein activity. However, features derived from evolutionary homology are not available for all proteins; and protein structural features are only available for a small fraction of proteins.

Coupling next generation sequencing with a mutagenesis screen allows parallel readout of tens of thousands of variants of a single protein (Fowler & Fields, 2014). The detail and coverage of these experiments provides a view into the mutational fitness landscape of individual proteins, giving quantitative relationships between sequence and protein function suitable for machine learning. We explore the possibility of adapting the Transformer to predict the quantitative effect of mutations.

We consider two settings for generalization of the information from large-scale mutagenesis data. The first is intra-protein variant effect prediction, where data from a limited sampling of mutations is used to predict the effect of unobserved mutations. This form of prediction is enabling for protein design and optimization applications, where repeated rounds of supervised training and prediction can guide an iterative exploration of the fitness landscape to design a biological property of a protein (Yang et al., 2019). The second setting is generalization to the mutational fitness landscape of a completely new protein for which the model has not received any prior quantitative mutation information.

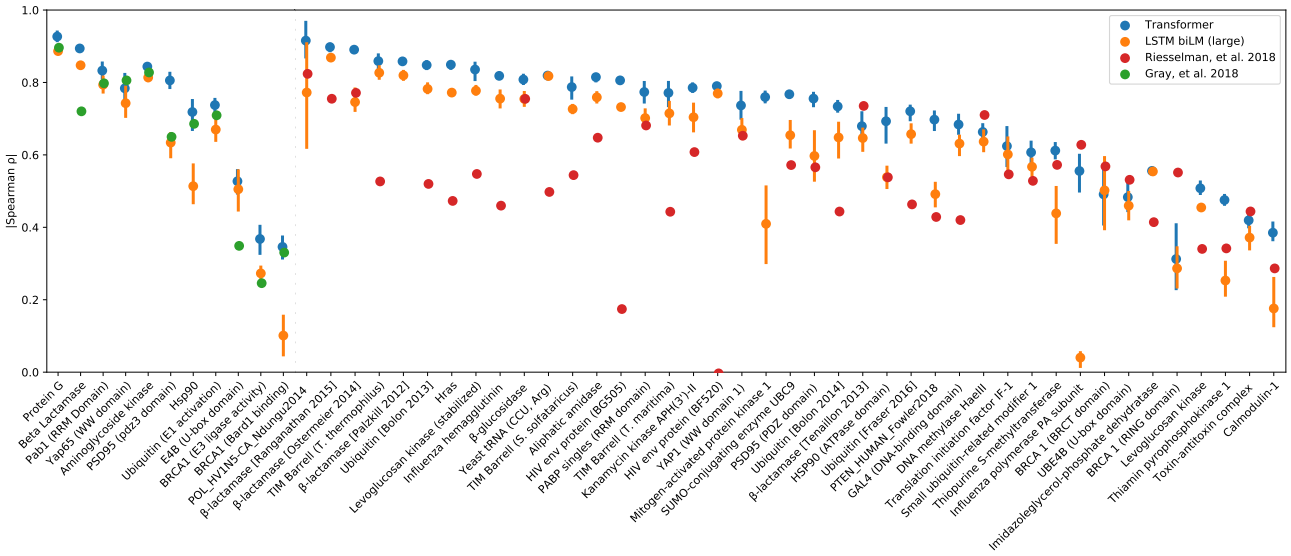

Figure 7. Representation learning enables state-of-the-art supervised prediction of the quantitative effect of mutations. Left panel: Envision dataset (Gray et al., 2018); right panel: DeepSequence dataset (Riesselman et al., 2018). Transformer representations (34-layer, UR50/S) are compared to the LSTM bidirectional language model (large model, UR50/S). The result of five-fold cross validation is reported for each protein. For each fold, supervised fine-tuning is performed on 80% of the mutational data for the protein, and results are evaluated on the remaining 20%. Transformer representations outperform baseline LSTM representations on both datasets. State-of-the-art methods are also shown for each dataset. Gray et al. (2018) is a supervised method using structural, evolutionary, and biochemical features, trained with the same protocol as used for the Transformer. Riesselman et al. (2018) is an unsupervised method trained on the MSA of each protein.

Intra-protein variant effect prediction We evaluate the representations on two deep mutational scanning datasets used by recent state-of-the-art methods for variant effect prediction, Envision (Gray et al., 2018) and DeepSequence (Riesselman et al., 2018). Collectively the data includes over 700,000 variant effect measurements from over 100 large-scale experimental mutagenesis datasets. Supervised methods have utility in protein engineering applications (Yang et al., 2018), therefore in the following experiments we evaluate by fine-tuning the Transformer-34 model with supervision from mutagenesis data.

Envision (Gray et al., 2018) relies on protein structural and evolutionary features to generalize. We explore whether the Transformer can achieve similar generalization results, without direct access to structural features. The same methodology for partitioning data for training and evaluation is used as in Gray et al. (2018) to allow a comparison of the results. Fine-tuning the Transformer pre-trained on UR50/S with variant activity data yields a mutational effect predictor which is comparable to the results of Envision while making predictions directly from protein sequences.

Figure 7 shows the fine-tuned Transformer exceeds the performance of Envision on 10 of the 12 proteins. For each protein a fraction $p = 0.8$ of the data is used for training and the remaining data is used for testing. We report mean and standard deviations for 5-fold cross-validation in Table S8. Results varying the fraction of data that is used for training are reported in Figure S4.

We also evaluate using the same five-fold cross validation methodology on the deep mutational scanning experiments assembled for DeepSequence (Riesselman et al., 2018). The fine-tuned Transformer model outperforms the fine-tuned LSTM baselines. While not directly comparable, we also include the performance of the original DeepSequence method which is unsupervised, and represents state-of-the-art in this setting.

Generalization to held-out proteins We analyze the Transformer's ability to generalize to the fitness landscape of a new protein. Following the protocol introduced in Envision, we use a leave-one-out analysis: to evaluate performance on a given protein, we train on data from the remaining $n - 1$ proteins and test on the held-out protein. Figure S5 shows that the Transformer's predictions from raw sequences perform better than Envision on 5 of the 9 tasks.

8. Related Work

Contemporaneously with the first preprint of this work, related preprints Alley et al. (2019), Heinzinger et al. (2019),

Model	Pre-Training	Params	RH	SSP	Contact
UniRep[1†]		18M	.527	58.4	21.9
SeqVec[2†]		93M	.545	62.1	29.0
Tape[3†]		38M	.581	58.0	23.2
LSTM biLM (S)	UR50/S	28.4M	.558	60.4	24.1
LSTM biLM (L)	UR50/S	113.4M	.574	62.4	27.8
Transformer-6	UR50/S	42.6M	**.653**	62.0	30.2
Transformer-12	UR50/S	85.1M	.639	65.4	37.7
Transformer-34	UR100	669.2M	.599	64.3	32.7
Transformer-34	UR50/S	669.2M	.639	**69.2**	**50.2**

Table 8. Comparison to related pre-training methods. (RH) Remote Homology at the fold level, using Hit-10 metric on SCOP. (SSP) Secondary structure Q8 accuracy on CB513. (Contact) Top-L long range contact precision on RaptorX test set from Wang et al. (2017). Results for additional test sets in Table S9. [1]Alley et al. (2019) [2]Heinzinger et al. (2019) [3]Rao et al. (2019). [†]The pre-training datasets for related work have differences from ours.

and Rao et al. (2019) explored language modeling for proteins, albeit at a smaller scale. These works also evaluated on a variety of downstream tasks. Alley et al. (2019) and Heinzinger et al. (2019) train LSTMs on UniRef50. Rao et al. (2019) trained a 12-layer Transformer model (38M parameters) on Pfam (Bateman et al., 2013). The baselines in this paper are comparable to these models.

We benchmark against related work in Table 8. Heinzinger et al. (2019), Alley et al. (2019), and Rao et al. (2019), evaluate models on differing downstream tasks and test sets. We retrieve the weights for the above models, evaluating them directly in our codebase against the panel of test sets used in this paper for remote homology, secondary structure prediction, and contact prediction, with the same training data and model architectures. This allows a direct comparison between the representations. Table 8 shows that high-capacity Transformers have strong performance for secondary structure and contact prediction significantly exceeding Alley et al. (2019), Heinzinger et al. (2019), and Rao et al. (2019). The small Transformer models trained as baselines also have higher performance than the methods with comparable parameter numbers.

Protein sequence embeddings have been the subject of recent investigation for protein engineering (Yang et al., 2018). Bepler & Berger (2019) investigated LSTM embeddings using supervision from protein structure. Since the preprint of this work appeared, related works have built on its exploration of protein sequence modeling, exploring generative models (Riesselman et al., 2019; Madani et al., 2020), internal representations of Transformers (Vig et al., 2020), and applications of representation learning and generative modeling such as classification (Elnaggar et al., 2019; Strodthoff et al., 2020), mutational effect prediction (Luo et al., 2020), and design of sequences (Repecka et al., 2019; Hawkins-Hooker et al., 2020; Amimeur et al., 2020).

9. Discussion

One of the goals for artificial intelligence in biology could be the creation of controllable predictive and generative models that can read and generate biology in its native language. Accordingly, research will be necessary into methods that can learn intrinsic biological properties directly from protein sequences, which can be transferred to prediction and generation.

We investigated deep learning across evolution at the scale of the largest protein sequence databases, training contextual language models across 86 billion amino acids from 250 million sequences. The space of representations learned from sequences by high-capacity networks reflects biological structure at multiple levels, including that of amino acids, proteins, and evolutionary homology. Information about secondary and tertiary structure is internalized and represented within the network. Knowledge of intrinsic biological properties emerges without supervision — no learning signal other than sequences is given during pre-training.

We find that networks that have been trained across evolutionary data generalize: information can be extracted from representations by linear projections, deep neural networks, or by adapting the model using supervision. Fine-tuning produces results that match state-of-the-art on variant activity prediction. Predictions are made directly from the sequence, using features that have been automatically learned by the language model, rather than selected by domain knowledge.

We find that pre-training discovers information that is not present in current state-of-the-art features. The learned features can be combined with features used by state-of-the-art

structure prediction methods to improve results. Empirically we find that features discovered by larger models perform better on downstream tasks. The Transformer outperforms LSTMs with similar capacity across benchmarks. Increasing diversity of the training data results in significant improvements to the representations.

While the contextual language models we study are of comparable scale to those used in the text domain, our experiments have not yet reached the limit of scale. We observed that even the highest capacity models we trained (with approximately 700M parameters) under-fit the 250M sequences, due to insufficient model capacity. The relationship we find between language modeling fidelity and the information in the learned representations suggests that higher capacity models will yield better representations. These findings imply potential for further model scale and data diversity incorporating sequences from metagenomics.

Combining high-capacity generative models with gene synthesis and high throughput characterization can enable generative biology. The network architectures we have trained can be used to generate new sequences (Wang & Cho, 2019). If neural networks can transfer knowledge learned from protein sequences to design functional proteins, this could be coupled with predictive models to jointly generate and optimize sequences for desired functions. The size of current sequence data and its projected growth point toward the possibility of a general purpose generative model that can condense the totality of sequence statistics, internalizing and integrating fundamental chemical and biological concepts including structure, function, activity, localization, binding, and dynamics, to generate new sequences that have not been seen before in nature but that are biologically active.

Pre-trained models

Transformer models and baselines are available at: `https://github.com/facebookresearch/esm`

Acknowledgments

We thank Tristan Bepler, Richard Bonneau, Yilun Du, Vladimir Gligorijevic, Anika Gupta, Omer Levy, Ian Peikon, Hetunandan Kamisetty, Laurens van der Maaten, Ethan Perez, Oded Regev, Neville Sanjana, and Emily Wang for feedback on the manuscript and insightful conversations. We thank Jinbo Xu for sharing RaptorX features and help with CASP13. We thank Michael Klausen for providing Netsurf training code. Alexander Rives was supported at NYU by NSF Grant #1339362.

References

Adzhubei, I., Jordan, D. M., and Sunyaev, S. R. Predicting functional effect of human missense mutations using polyphen-2. *Current protocols in human genetics*, 76(1): 7–20, 2013.

Alley, E. C., Khimulya, G., Biswas, S., AlQuraishi, M., and Church, G. M. Unified rational protein engineering with sequence-based deep representation learning. *Nature methods*, 16(12):1315–1322, 2019.

Altschuh, D., Lesk, A., Bloomer, A., and Klug, A. Correlation of co-ordinated amino acid substitutions with function in viruses related to tobacco mosaic virus. *Journal of Molecular Biology*, 193(4):693–707, 1987. ISSN 0022-2836. doi: 10.1016/0022-2836(87)90352-4.

Altschuh, D., Vernet, T., Berti, P., Moras, D., and Nagai, K. Coordinated amino acid changes in homologous protein families. *Protein Engineering, Design and Selection*, 2 (3):193–199, 1988.

Altschul, S. F. and Koonin, E. V. Iterated profile searches with psi-blast – a tool for discovery in protein databases. *Trends in Biochemical Sciences*, 23(11):444–447, 11 1998. ISSN 0968-0004. doi: 10.1016/S0968-0004(98)01298-5.

Altschul, S. F., Gish, W., Miller, W., Myers, E. W., and Lipman, D. J. Basic local alignment search tool. *Journal of Molecular Biology*, 215(3):403–410, 1990. ISSN 0022-2836. doi: 10.1016/S0022-2836(05)80360-2.

Amimeur, T., Shaver, J. M., Ketchem, R. R., Taylor, J. A., Clark, R. H., Smith, J., Van Citters, D., Siska, C. C., Smidt, P., Sprague, M., et al. Designing feature-controlled humanoid antibody discovery libraries using generative adversarial networks. *bioRxiv*, 2020.

Anishchenko, I., Ovchinnikov, S., Kamisetty, H., and Baker, D. Origins of coevolution between residues distant in protein 3d structures. *Proceedings of the National Academy of Sciences*, 114(34):9122–9127, 2017.

Baevski, A., Edunov, S., Liu, Y., Zettlemoyer, L., and Auli, M. Cloze-driven pretraining of self-attention networks. *CoRR*, abs/1903.07785, 2019. URL `http://arxiv.org/abs/1903.07785`.

Balakrishnan, S., Kamisetty, H., Carbonell, J. G., Lee, S.-I., and Langmead, C. J. Learning generative models for protein fold families. *Proteins: Structure, Function, and Bioinformatics*, 79(4):1061–1078, 2011.

Bateman, A., Heger, A., Sonnhammer, E. L. L., Mistry, J., Clements, J., Tate, J., Hetherington, K., Holm, L., Punta, M., Coggill, P., Eberhardt, R. Y., Eddy, S. R., and

Finn, R. D. Pfam: the protein families database. *Nucleic Acids Research*, 42(D1):D222–D230, 11 2013. ISSN 0305-1048. doi: 10.1093/nar/gkt1223.

Bengio, Y., Ducharme, R., Vincent, P., and Jauvin, C. A neural probabilistic language model. *Journal of machine learning research*, 3(Feb):1137–1155, 2003.

Bepler, T. and Berger, B. Learning protein sequence embeddings using information from structure. In *International Conference on Learning Representations*, 2019. URL https://openreview.net/forum?id=SygLehCqtm.

Bycroft, C., Freeman, C., Petkova, D., Band, G., Elliott, L. T., Sharp, K., Motyer, A., Vukcevic, D., Delaneau, O., O'Connell, J., et al. The uk biobank resource with deep phenotyping and genomic data. *Nature*, 562(7726):203, 2018.

Collobert, R. and Weston, J. A unified architecture for natural language processing: Deep neural networks with multitask learning. In *Proceedings of the 25th international conference on Machine learning*, pp. 160–167. ACM, 2008.

Cosgrove, M. S., Naylor, C., Paludan, S., Adams, M. J., and Levy, H. R. On the mechanism of the reaction catalyzed by glucose 6-phosphate dehydrogenase,. *Biochemistry*, 37(9):2759–2767, 03 1998. ISSN 0006-2960. doi: 10.1021/bi972069y.

Cuff, J. A. and Barton, G. J. Evaluation and improvement of multiple sequence methods for protein secondary structure prediction. *Proteins: Structure, Function, and Bioinformatics*, 34(4):508–519, 1999.

Dai, A. M. and Le, Q. V. Semi-supervised sequence learning. In *Advances in Neural Information Processing Systems*, pp. 3079–3087, 2015.

Devlin, J., Chang, M., Lee, K., and Toutanova, K. BERT: pre-training of deep bidirectional transformers for language understanding. *CoRR*, abs/1810.04805, 2018. URL http://arxiv.org/abs/1810.04805.

Dunbrack Jr, R. L. Sequence comparison and protein structure prediction. *Current opinion in structural biology*, 16 (3):374–384, 2006.

Eddy, S. R. Profile hidden markov models. *Bioinformatics*, 14(9):755–763, 10 1998. ISSN 1367-4803. doi: 10.1093/bioinformatics/14.9.755.

Ekeberg, M., Lövkvist, C., Lan, Y., Weigt, M., and Aurell, E. Improved contact prediction in proteins: Using pseudolikelihoods to infer potts models. *Phys. Rev. E*, 87:012707, Jan 2013a. doi: 10.1103/PhysRevE.87.012707. URL https://link.aps.org/doi/10.1103/PhysRevE.87.012707.

Ekeberg, M., Lövkvist, C., Lan, Y., Weigt, M., and Aurell, E. Improved contact prediction in proteins: using pseudolikelihoods to infer potts models. *Physical Review E*, 87(1):012707, 2013b.

Elnaggar, A., Heinzinger, M., Dallago, C., and Rost, B. End-to-end multitask learning, from protein language to protein features without alignments. *bioRxiv*, pp. 864405, 2019.

Fowler, D. M. and Fields, S. Deep mutational scanning: a new style of protein science. *Nature methods*, 11(8):801, 2014.

Fox, N. K., Brenner, S. E., and Chandonia, J.-M. Scope: Structural classification of proteins—extended, integrating scop and astral data and classification of new structures. *Nucleic acids research*, 42(D1):D304–D309, 2013.

Gabaldon, T. Evolution of proteins and proteomes: a phylogenetics approach. *Evol Bioinform Online*, 1:51–61, 2007.

Göbel, U., Sander, C., Schneider, R., and Valencia, A. Correlated mutations and residue contacts in proteins. *Proteins: Structure, Function, and Bioinformatics*, 18(4):309–317, 1994.

Gray, V. E., Hause, R. J., Luebeck, J., Shendure, J., and Fowler, D. M. Quantitative missense variant effect prediction using large-scale mutagenesis data. *Cell systems*, 6(1):116–124, 2018.

Harris, Z. S. Distributional structure. *Word*, 10(2-3):146–162, 1954.

Hawkins-Hooker, A., Depardieu, F., Baur, S., Couairon, G., Chen, A., and Bikard, D. Generating functional protein variants with variational autoencoders. *BioRxiv*, 2020.

Hecht, M., Bromberg, Y., and Rost, B. Better prediction of functional effects for sequence variants. *BMC genomics*, 16(8):S1, 2015.

Heinzinger, M., Elnaggar, A., Wang, Y., Dallago, C., Nechaev, D., Matthes, F., and Rost, B. Modeling aspects of the language of life through transfer-learning protein sequences. *BMC bioinformatics*, 20(1):723, 2019.

Hoffmann, B., Konrat, R., Bothe, H., Buckel, W., and Kräutler, B. Structure and dynamics of the b12-binding subunit of glutamate mutase from clostridium cochlearium. *European journal of biochemistry*, 263(1):178–188, 1999.

Hopf, T., Ingraham, J., Poelwijk, F., Scharfe, C., Springer, M., Sander, C., and Marks, D. Mutation effects predicted from sequence co-variation. *Nature Biotechnology*, 35: 128–135, 1 2017.

Hormoz, S. Amino acid composition of proteins reduces deleterious impact of mutations. *Scientific reports*, 3: 2919, 2013.

Huerta-Cepas, J., Forslund, S. K., Bork, P., Hernández-Plaza, A., von Mering, C., Szklarczyk, D., Heller, D., Cook, H., Jensen, L., Mende, D. R., Letunic, I., and Rattei, T. eggNOG 5.0: a hierarchical, functionally and phylogenetically annotated orthology resource based on 5090 organisms and 2502 viruses. *Nucleic Acids Research*, 47(D1):D309–D314, 11 2018. ISSN 0305-1048. doi: 10.1093/nar/gky1085.

Jarrett, K., Kavukcuoglu, K., Ranzato, M., and LeCun, Y. What is the best multi-stage architecture for object recognition? In *2009 IEEE 12th international conference on computer vision*, pp. 2146–2153. IEEE, 2009.

Johnson, J., Douze, M., and Jégou, H. Billion-scale similarity search with gpus. *CoRR*, abs/1702.08734, 2017. URL http://arxiv.org/abs/1702.08734.

Jones, D. T. and Kandathil, S. M. High precision in protein contact prediction using fully convolutional neural networks and minimal sequence features. *Bioinformatics*, 34(19):3308–3315, 2018.

Jones, D. T., Buchan, D. W., Cozzetto, D., and Pontil, M. Psicov: precise structural contact prediction using sparse inverse covariance estimation on large multiple sequence alignments. *Bioinformatics*, 28(2):184–190, 2011.

Karczewski, K. J., Francioli, L. C., Tiao, G., Cummings, B. B., Alföldi, J., Wang, Q., Collins, R. L., Laricchia, K. M., Ganna, A., Birnbaum, D. P., et al. Variation across 141,456 human exomes and genomes reveals the spectrum of loss-of-function intolerance across human protein-coding genes. *BioRxiv*, pp. 531210, 2019.

Kato, M., Shimizu, T., Mizuno, T., and Hakoshima, T. Structure of the histidine-containing phosphotransfer (hpt) domain of the anaerobic sensor protein arcb complexed with the chemotaxis response regulator chey. *Acta Crystallographica Section D*, 55(7):1257–1263, 07 1999. doi: 10.1107/S0907444999005053.

Kim, Y., Jernite, Y., Sontag, D., and Rush, A. M. Character-aware neural language models. In *Proceedings of the Thirtieth AAAI Conference on Artificial Intelligence, February 12-17, 2016, Phoenix, Arizona, USA.*, pp. 2741–2749, 2016. URL http://www.aaai.org/ocs/index.php/AAAI/AAAI16/paper/view/12489.

Klausen, M. S., Jespersen, M. C., Nielsen, H., Jensen, K. K., Jurtz, V. I., Sonderby, C. K., Sommer, M. O. A., Winther, O., Nielsen, M., Petersen, B., and Marcatili, P. NetSurfP-2.0: Improved prediction of protein structural features by integrated deep learning. *Proteins*, 87(6):520–527, 06 2019.

Kondrashov, F. A., Bork, P., Sunyaev, S., and Ramensky, V. Impact of selection, mutation rate and genetic drift on human genetic variation. *Human Molecular Genetics*, 12(24):3325–3330, 12 2003. ISSN 0964-6906. doi: 10.1093/hmg/ddg359. URL https://doi.org/10.1093/hmg/ddg359.

Kryshtafovych, A., Schwede, T., Topf, M., Fidelis, K., and Moult, J. Critical assessment of methods of protein structure prediction (casp)—round xiii. *Proteins: Structure, Function, and Bioinformatics*, 87(12):1011–1020, 2019.

Kumar, P., Henikoff, S., and Ng, P. C. Predicting the effects of coding non-synonymous variants on protein function using the sift algorithm. *Nature protocols*, 4(7):1073, 2009.

Lek, M., Karczewski, K. J., Minikel, E. V., Samocha, K. E., Banks, E., Fennell, T., O'Donnell-Luria, A. H., Ware, J. S., Hill, A. J., Cummings, B. B., et al. Analysis of protein-coding genetic variation in 60,706 humans. *Nature*, 536(7616):285, 2016.

Levitt, M. Conformational preferences of amino acids in globular proteins. *Biochemistry*, 17(20):4277–4285, 1978.

Luo, Y., Vo, L., Ding, H., Su, Y., Liu, Y., Qian, W. W., Zhao, H., and Peng, J. Evolutionary context-integrated deep sequence modeling for protein engineering. In *International Conference on Research in Computational Molecular Biology*, pp. 261–263. Springer, 2020.

Ma, J., Wang, S., Wang, Z., and Xu, J. Mrfalign: protein homology detection through alignment of markov random fields. In *International Conference on Research in Computational Molecular Biology*, pp. 173–174. Springer, 2014.

Maaten, L. v. d. and Hinton, G. Visualizing data using t-sne. *Journal of machine learning research*, 9(Nov): 2579–2605, 2008.

Madani, A., McCann, B., Naik, N., Keskar, N. S., Anand, N., Eguchi, R. R., Huang, P.-S., and Socher, R. Progen: Language modeling for protein generation. *arXiv preprint arXiv:2004.03497*, 2020.

Marks, D. S., Colwell, L. J., Sheridan, R., Hopf, T. A., Pagnani, A., Zecchina, R., and Sander, C. Protein 3d structure computed from evolutionary sequence variation. *PloS one*, 6(12):e28766, 2011.

Mikolov, T., Sutskever, I., Deoras, A., Le, H.-S., Kombrink, S., and Cernocky, J. Subword language modeling with neural networks. *preprint (http://www. fit. vutbr. cz/imikolov/rnnlm/char. pdf)*, 8, 2012.

Mikolov, T., Chen, K., Corrado, G., and Dean, J. Efficient estimation of word representations in vector space. In *1st International Conference on Learning Representations, ICLR 2013, Scottsdale, Arizona, USA, May 2-4, 2013, Workshop Track Proceedings*, 2013. URL http://arxiv.org/abs/1301.3781.

Morcos, F., Pagnani, A., Lunt, B., Bertolino, A., Marks, D. S., Sander, C., Zecchina, R., Onuchic, J. N., Hwa, T., and Weigt, M. Direct-coupling analysis of residue coevolution captures native contacts across many protein families. *Proceedings of the National Academy of Sciences*, 108(49):E1293–E1301, 2011.

Moult, J., Fidelis, K., Kryshtafovych, A., Schwede, T., and Tramontano, A. Critical assessment of methods of protein structure prediction: Progress and new directions in round xi. *Proteins: Structure, Function, and Bioinformatics*, 84: 4–14, 2016.

Moult, J., Fidelis, K., Kryshtafovych, A., Schwede, T., and Tramontano, A. Critical assessment of methods of protein structure prediction (casp)—round xii. *Proteins: Structure, Function, and Bioinformatics*, 86:7–15, 2018.

Orengo, C. A., Michie, A., Jones, S., Jones, D. T., Swindells, M., and Thornton, J. M. Cath–a hierarchic classification of protein domain structures. *Structure*, 5(8):1093–1109, 1997.

Overbaugh, J. and Bangham, C. Selection forces and constraints on retroviral sequence variation. *Science*, 292: 1106–1109, 5 2001. doi: 10.1126/science.1059128.

Peters, M. E., Neumann, M., Iyyer, M., Gardner, M., Clark, C., Lee, K., and Zettlemoyer, L. Deep contextualized word representations. In *Proceedings of the 2018 Conference of the North American Chapter of the Association for Computational Linguistics: Human Language Technologies, NAACL-HLT 2018, New Orleans, Louisiana, USA, June 1-6, 2018, Volume 1 (Long Papers)*, pp. 2227–2237, 2018. URL https://aclanthology.info/papers/N18-1202/n18-1202.

Radford, A., Narasimhan, K., Salimans, T., and Sutskever, I. Improving language understanding by generative pre-training. 2018.

Radford, A., Wu, J., Child, R., Luan, D., Amodei, D., and Sutskever, I. Language models are unsupervised multitask learners. 2019.

Rao, R., Bhattacharya, N., Thomas, N., Duan, Y., Chen, P., Canny, J., Abbeel, P., and Song, Y. Evaluating protein transfer learning with tape. In *Advances in Neural Information Processing Systems*, pp. 9686–9698, 2019.

Remmert, M., Biegert, A., Hauser, A., and Söding, J. Hhblits: lightning-fast iterative protein sequence searching by hmm-hmm alignment. *Nature Methods*, 9:173 EP, 12 2011. doi: 10.1038/nmeth.1818.

Rentzsch, P., Witten, D., Cooper, G. M., Shendure, J., and Kircher, M. Cadd: predicting the deleteriousness of variants throughout the human genome. *Nucleic acids research*, 47(D1):D886–D894, 2018.

Repecka, D., Jauniskis, V., Karpus, L., Rembeza, E., Zrimec, J., Poviloniene, S., Rokaitis, I., Laurynenas, A., Abuajwa, W., Savolainen, O., et al. Expanding functional protein sequence space using generative adversarial networks. *bioRxiv*, pp. 789719, 2019.

Riesselman, A. J., Ingraham, J. B., and Marks, D. S. Deep generative models of genetic variation capture the effects of mutations. *Nature Methods*, 15(10):816–822, 2018. ISSN 1548-7105. doi: 10.1038/s41592-018-0138-4.

Riesselman, A. J., Shin, J.-E., Kollasch, A. W., McMahon, C., Simon, E., Sander, C., Manglik, A., Kruse, A. C., and Marks, D. S. Accelerating protein design using autoregressive generative models. *bioRxiv*, pp. 757252, 2019.

Senior, A., Jumper, J., and Hassabis, D. AlphaFold: Using AI for scientific discovery, 12 2018. URL https://deepmind.com/blog/alphafold/.

Slaymaker, I. M., Gao, L., Zetsche, B., Scott, D. A., Yan, W. X., and Zhang, F. Rationally engineered cas9 nucleases with improved specificity. *Science*, 351(6268): 84–88, 2016. ISSN 0036-8075. doi: 10.1126/science.aad5227. URL https://science.sciencemag.org/content/351/6268/84.

Strodthoff, N., Wagner, P., Wenzel, M., and Samek, W. Udsmprot: universal deep sequence models for protein classification. *Bioinformatics*, 36(8):2401–2409, 2020.

Suzek, B. E., Huang, H., McGarvey, P., Mazumder, R., and Wu, C. H. UniRef: comprehensive and non-redundant UniProt reference clusters. *Bioinformatics*, 23(10):1282–1288, May 2007. ISSN 1367-4803. doi: 10.1093/bioinformatics/btm098. URL https://academic.oup.com/bioinformatics/article/23/10/1282/197795.

Suzek, B. E., Wang, Y., Huang, H., McGarvey, P. B., Wu, C. H., and Consortium, U. Uniref clusters: a comprehensive and scalable alternative for improving sequence similarity searches. *Bioinformatics*, 31(6):926–932, 2015.

The UniProt Consortium. The universal protein resource (uniprot). *Nucleic Acids Research*, 36(suppl_1):D190–D195, 11 2007. ISSN 0305-1048. doi: 10.1093/nar/gkm895.

Vaswani, A., Shazeer, N., Parmar, N., Uszkoreit, J., Jones, L., Gomez, A. N., Kaiser, Ł., and Polosukhin, I. Attention is all you need. In *Advances in neural information processing systems*, pp. 5998–6008, 2017.

Vig, J., Madani, A., Varshney, L. R., Xiong, C., Socher, R., and Rajani, N. F. Bertology meets biology: Interpreting attention in protein language models. *arXiv preprint arXiv:2006.15222*, 2020.

Wang, A. and Cho, K. BERT has a mouth, and it must speak: BERT as a markov random field language model. *CoRR*, abs/1902.04094, 2019. URL http://arxiv.org/abs/1902.04094.

Wang, S., Peng, J., Ma, J., and Xu, J. Protein secondary structure prediction using deep convolutional neural fields. *Scientific Reports*, 6, Jan 2016. URL https://doi.org/10.1038/srep18962. Article.

Wang, S., Sun, S., Li, Z., Zhang, R., and Xu, J. Accurate de novo prediction of protein contact map by ultra-deep learning model. *PLoS computational biology*, 13(1): e1005324, 2017.

Wang, S.-W., Bitbol, A.-F., and Wingreen, N. Revealing evolutionary constraints on proteins through sequence analysis. *PLoS Comput Biol*, 15(4), 2019. doi: 10.1371/journal.pcbi.1007010.

Weigt, M., White, R. A., Szurmant, H., Hoch, J. A., and Hwa, T. Identification of direct residue contacts in protein–protein interaction by message passing. *Proceedings of the National Academy of Sciences*, 106(1):67–72, 2009.

Xu, J. Distance-based protein folding powered by deep learning. *arXiv preprint arXiv:1811.03481*, 2018.

Yang, K. K., Wu, Z., Bedbrook, C. N., and Arnold, F. H. Learned protein embeddings for machine learning. *Bioinformatics*, 34(15):2642–2648, 2018.

Yang, K. K., Wu, Z., and Arnold, F. H. Machine-learning-guided directed evolution for protein engineering. *Nature methods*, 16(8):687–694, 2019.

Yanofsky, C., Horn, V., and Thorpe, D. Protein structure relationships revealed by mutational analysis. *Science*, 146(3651):1593–1594, 1964.

Zhou, J. and Troyanskaya, O. G. Deep supervised and convolutional generative stochastic network for protein secondary structure prediction. In *Proceedings of the 31th International Conference on Machine Learning, ICML 2014, Beijing, China, 21-26 June 2014*, pp. 745–753, 2014. URL http://jmlr.org/proceedings/papers/v32/zhou14.html.

Approach & Data

1. Methodology

Formally the evaluation of pre-trained models proceeds in the setting of inductive semi-supervised learning (Chapelle et al., 2006). We assume a data density $p(x)$ and a joint distribution of data and labels $p(x, y)$. In supervised learning the goal is to estimate $p(y|x)$; typically many samples are necessary. Here with limited information about labels, the model relies on structure learned from $p(x)$ to generalize. Unsupervised representation learning using deep neural networks (Hinton & Salakhutdinov, 2006) has been effective for generalization in this setting.

The experiments have two stages. First a model is pre-trained with an unsupervised objective on protein sequences. The model produces a set of features $F(x)$. Then supervision is applied to train a second model to predict $p(y|x)$ for a downstream task, replacing the raw sequence x with the learned features $F(x)$. Substituting $p(y|F(x))$ for $p(y|x)$ will improve the model if $F(x)$ identifies useful features. The representations can be kept frozen, or fine-tuned by optimizing the parameters of $F(x)$ with the supervised objective.

To evaluate performance on secondary and tertiary structure prediction, we rely on two hold-out strategies: (i) sequence identity hold-out, where related sequences are excluded from training data using an identity threshold; and (ii) temporal hold-out, where training and test data are strictly separated by a temporal cutoff. For contact prediction, CASP13 (Kryshtafovych et al., 2019) evaluations use a temporal hold-out for both pre-training and downstream supervision; CASP12 (Moult et al., 2018) evaluations use a temporal hold-out for downstream supervision, but not pre-training; RaptorX Test (Wang et al., 2017) and CASP11 (Moult et al., 2016) evaluations use a sequence identity hold-out at 25% identity. For secondary structure prediction, CASP13 uses a temporal hold-out for both pre-training and downstream supervision; and CB513 (Cuff & Barton, 1999) uses a sequence identity hold-out at 25% identity.

The evaluations in this paper use the labeled and unlabeled data in a manner analogous to classical computational biology methods exploiting large sequence databases at test time. Sequence search underlies many classical and state-of-the-art approaches to biological prediction. Structural and functional properties can be imputed by sequence homology (Eddy, 1998; Söding, 2004). Single-family generative models fit parametric distributions to MSA data (Weigt et al., 2009; Marks et al., 2011; Morcos et al., 2011; Jones et al., 2011; Balakrishnan et al., 2011; Ekeberg et al., 2013). These methods seek to exploit the information in the unlabeled data of sequences to infer useful structure. Typically during test time homology-based methods are afforded access to the sequence database. Similarly, in our work, the model is pre-trained on the sequence database, and the test time predictor is afforded information learned from the database through the pre-trained representations. Accordingly in this work, unsupervised pre-training aims to learn from the dependencies and variations among related, as well as very different, sequences to develop a common representation through a generative model that explains their variations. The distinction in this paper is that instead of training a parametric model on a single family of related sequences, a single model is trained across all sequences. The model thereby proposes to capture and represent dependencies that extend beyond the single sequence family level to the full variation in the sequence database.

2. Pre-training datasets

UniParc pre-training dataset. A series of development models are trained on UniParc (The UniProt Consortium, 2007) Release 2019_01 which contains approximately 250M sequences. 1M sequences are held-out randomly for validation. These models were used in the preprint of this paper, and representations from the models are visualized in Figures 2, 4, and 5.

UniRef pre-training datasets. Datasets are based on UniRef (Suzek et al., 2015) dated March 28, 2018 to permit a temporal hold-out with CASP13. 10% of UniRef50 clusters are randomly selected as a held-out evaluation set, yielding 3.02 million representative sequences for evaluation. Three training datasets are used, removing all sequences belonging to clusters selected for the evaluation set: (i) UR100, 124.9M UniRef100 representative sequences; (ii) UR50/S, 27.1M UniRef50 representative sequences; (iii) UR50/D, 124.9M UniRef50 cluster members sampled evenly by cluster. To ensure a deterministic validation set, we removed sequences longer than 1024 amino acids from the validation set.

3. Downstream tasks

Remote Homology. A dataset of remote homolog pairs is derived from SCOP (Fox et al., 2014) containing 256,806 pairs of remote homologs at the fold level and 92,944 at the superfamily level, consisting of 217 unique folds and 366 unique superfamilies. Creation of the dataset is detailed below in the section on remote homology.

Linear projections. Secondary structure projections are evaluated on CB513 (Cuff & Barton, 1999) using the training set of 5,365 examples from Zhou & Troyanskaya (2014) with sequence identity hold-out at 25% identity. Residue-residue contact projections are evaluated on a dataset derived from CATH S40 (Orengo et al., 1997), consisting of 3,339

test domains and 18,696 training domains with sequence identity hold-out at 20% identity.

Secondary structure prediction. All downstream models are trained using the Netsurf (Klausen et al., 2019) training dataset containing 10,837 examples. Netsurf features are replicated using MMseqs2 (Steinegger & Söding, 2017) on the Uniclust90 (Mirdita et al., 2017) dataset released April 2017. For test sets we use (i) the standard CB513 (Cuff & Barton, 1999) test set of 513 sequences with sequence identity hold-out at 25% identity; and (ii) the 34 publicly available CASP domains, using DSSP (Kabsch & Sander, 1983) to label secondary structure, with temporal hold-out for both pre-training and downstream data.

Contact prediction. All downstream models are trained using the training and test sets of Wang et al. (2017). Comparisons with RaptorX features use features from Wang et al. (2017) and Xu (2018). The following test sets are used: (i) RaptorX Test, 500 domains (25% sequence identity hold-out); (ii) CASP11, 105 domains (25% sequence identity hold-out); (iii) CASP12, 55 domains (temporal hold-out from training data but not pre-training data); (iv) CASP13, 34 publicly released domains (temporal hold-out from training data and pre-training data). The training set consists of 6,767 sequences with contact map targets, a subset of PDB created in February 2015 (Wang et al., 2017). The use of an earlier version of the PDB ensures a temporal hold-out w.r.t. both CASP12 and CASP13. Additionally, Wang et al. (2017) implemented a sequence identity hold-out for Test and CASP11 by removing proteins from the training set which share >25% sequence identity or have BLAST E-value <0.1 with the proteins in these test sets.

Mutational effect prediction. The model is fine-tuned on deep mutational scanning datasets compiled by Gray et al. (2018) and Riesselman et al. (2018).

4. Background on language models and embeddings

Deep language models are parametric functions that map sequences into distributed word representations in a learned vector space (Bengio et al., 2003; Mikolov et al., 2013a;b; Pennington et al., 2014; Lample et al., 2017). These vectors, called embeddings, distribute the meaning of the source sequence across multiple components of the vector, such that semantically similar objects are mapped to nearby vectors in representation space.

Recently, results of large-scale pre-trained language models have advanced the field of natural language processing and impacted the broader deep learning community. Peters et al. (2018) used a coupled language model objective to train bidirectional LSTMs in order to extract context dependent word embeddings. These embeddings showed improvement for a range of NLP tasks. Radford et al. (2018) explored a semi-supervised method using left-to-right Transformer models to learn universal representations using unsupervised pre-training, followed by fine-tuning on specific downstream tasks. Recently, Devlin et al. (2018) proposed BERT to pre-train deep representations using bidirectional Transformer models. They proposed a pre-training objective based on masked language modeling, which allowed capturing both left and right contexts to obtain deep bidirectional token representations, and obtained state-of-the-art results on 11 downstream language understanding tasks, such as question answering and natural language inference, without substantial task-specific architecture modifications. Radford et al. (2019) extended their earlier work and proposed GPT-2, highlighting the importance of scale along dimensions of number of model parameters and size of pre-training data, and demonstrated their learned language model is able to achieve surprisingly good results on various NLP tasks without task-specific training. Analogous follow-up work on other domains have also shown promising results (Sun et al., 2019).

5. The Transformer

We use a deep bidirectional Transformer encoder model (Devlin et al., 2018; Vaswani et al., 2017) and process data at the character-level, corresponding to individual amino-acids in our application. In contrast to models that are based on recurrent or convolutional neural networks, the Transformer makes no assumptions on the ordering of the input and instead uses position embeddings. Particularly relevant to protein sequences is the Transformer's natural ability to model long range dependencies, which are not effectively captured by RNNs or LSTMs (Khandelwal et al., 2018). One key factor affecting the performance of LSTMs on these tasks is the path lengths that must be traversed by forward activation and backward gradient signals in the network (Hochreiter et al., 2001). It is well known that structural properties of protein sequences are reflected in long-range dependencies (Kihara, 2005). Classical methods that aim to detect pairwise dependencies in multiple sequence alignments are able to model entire sequences. Similarly, the Transformer builds up a representation of a sequence by alternating self-attention with non-linear projections. self-attention structures computation so that each position is represented by a weighted sum of the other positions in the sequence. The attention weights are computed dynamically and allow each position to choose what information from the rest of the sequence to integrate at every computation step.

Developed to model large contexts and long range dependencies in language data, self-attention architectures currently give state-of-the-art performance on various natural language tasks, mostly due to the Transformer's scalability in parameters and the amount of context it can integrate (De-

vlin et al., 2018). The tasks include token-level tasks like part-of-speech tagging, sentence-level tasks such as textual entailment, and paragraph-level tasks like question-answering.

Scaled dot-product attention. Self-attention takes a sequence of vectors $(h_1, \ldots, h_n)$ and produces a sequence of vectors $(h'_1, \ldots, h'_n)$ by computing interactions between all elements in the sequence. The Transformer model uses scaled dot-product attention (Vaswani et al., 2017):

$$A(h) = \text{softmax}(1/\sqrt{d}\, Q(h)K(h)^T)V(h) \quad (2)$$

Here the query Q, key K, and value V, are projections of the input sequence to $n \times d$ matrices where n is the length of the sequence and d is the inner dimension of the matrix outer product between Q and K. This outer product parameterizes an $n \times n$ map of attention logits, which are rescaled, and passed through the softmax function row-wise, thereby representing each position of the sequence in the output as a convex combination of the sequence of values V. One step of self-attention directly models possible pairwise interactions between all positions in the sequence simultaneously. Note the contrast to recurrent and convolutional models which can only represent long-range context through many steps, and the parallel in inductive bias with the explicit pairwise parameterization of Markov Random Fields (Weigt et al., 2009; Marks et al., 2011; Morcos et al., 2011; Jones et al., 2011; Balakrishnan et al., 2011; Ekeberg et al., 2013) in widespread use for modeling protein MSAs.

Multi-headed self-attention concatenates the output of t independent attention heads:

$$A_{\text{MH}}(x) = A_1(x) \ldots A_t(x) \quad (3)$$

Use of multiple heads enables representation of different inter-position interaction patterns.

Architecture The Transformer models (Vaswani et al., 2017) in this work take a sequence of tokens $(x_1, \ldots, x_n)$ and output a sequence of log probabilities $(y_1, \ldots, y_n)$ which are optimized using the masked language modeling objective. The computation proceeds through a series of residual blocks producing hidden states, each a sequence of vectors $(h_1, \ldots, h_n)$ with embedding dimension d.

The Transformer model architecture consists of a series of encoder blocks interleaving two functions: a multi-headed self-attention computing position-position interactions across the sequence, and a feed-forward network applied independently at each position.

The attention unit:

$$U_{\text{AT}}(h) = P(A_{\text{MH}}(n(h))) \quad (4)$$

Applies one step of multi-headed scaled dot-product attention to the normalized input, denoted by $n(x)$, projecting the result into the residual path.

The feed-forward network (with the output state of P_1 defining the "MLP dimension"):

$$U_{\text{FF}}(h) = P_2(g(P_1(n(h))) \quad (5)$$

Passes the normalized input through a position-independent multi-layered perceptron (MLP) with activation function $g(x)$.

The full Transformer block:

$$\begin{aligned} &B(h): \\ &\quad h \leftarrow h + U_{\text{AT}}(h) \\ &\quad h \leftarrow h + U_{\text{FF}}(h) \end{aligned}$$

Successively applies the self-attention unit, and the feed-forward network on a residual path.

The Transformer model:

$$\begin{aligned} &\text{Transformer}(x): \\ &\quad h \leftarrow E(x) + H(x) \\ &\quad h \leftarrow B_k(h) \;\; \text{for } k \in 1 \ldots K \\ &\quad y \leftarrow W(h) \end{aligned}$$

Consists of an embedding step with token $E(x)$ and positional $H(x)$ embeddings, followed by K layers of Transformer blocks, before a projection W to log probabilities. The raw input sequence is represented as a sequence of 1-hot vectors of dimension 25, which is passed through $E(x)$ the learned embedding layer before being presented to the first Transformer layer.

The models trained in the paper use pre-activation blocks (He et al., 2016), where the layer normalization (Ba et al., 2016) is applied prior to the activation as in Radford et al. (2019), enabling stable training of deep Transformer networks. No dropout is used. All projections include biases, except for the token and positional embeddings. We use learned token embeddings, and harmonic positional embeddings as in (Vaswani et al., 2017). The feed-forward network uses the Gaussian error linear unit (Hendrycks & Gimpel, 2016) activation function. We initialize all layers from a zero centered normal distribution with standard deviation 0.02, and re-scale the initialization of the projections into the residual path by $1/\sqrt{L}$ where L is the number of residual layers. All biases are initialized to zero. The query, key, and value projections are to d dimensions, and the hidden dimension of the feed-forward network is $4d$.

6. Pre-trained Transformer Models

UniParc development models We experimented with Transformer models of various depths, including a 36-layer

# Layers	# Heads	Embedding Dim	MLP Dim	# Params	Steps (A)	Steps (B)
12	12	768	3072	85.1M	1.5M	1.6M
24	12	768	3072	170.2M	220k	300k
36	20	1280	5120	708.6M	200k	300k

Table S1. Hyperparameters for development Transformer models trained on UniParc. Embedding dim is the dimension of the hidden states at the output of each transformer block. MLP Dim refers to the width of hidden layer P_1 in the Transformer's MLPs. (A) refers to the number of pre-training steps before analyzing secondary structure by linear projection. (B) gives the number of pre-training steps before visualizations were performed, and for analysis of residue-residue contacts in Figure S6.

# Layers	# Heads	Embedding Dim	MLP Dim	# Params	Data	Steps
6	12	768	3072	42.6M	UR50/S	840K
12	12	768	3072	85.1M	UR50/S	840K
34	20	1280	5120	669.2M	UR100	275K
34	20	1280	5120	669.2M	UR50/S	840K
34	20	1280	5120	669.2M	UR50/D	906K

Table S2. Hyperparameters for UniRef Transformer models. Note: UR100 model stopped making significant progress on valid loss and was stopped at 275K updates.

Transformer with 708.6 million parameters, and a 12-layer model with 85.1M parameters trained. Development models were trained on UniParc, and used for visualizations and analysis by linear projections. Details are in Table S1.

UniRef models We train 34-layer models with 669.2M parameters across different datasets and fractions of training data. Additionally we train 6 and 12-layer models. These models are detailed in Table S2.

Pre-training task The masked language modeling pre-training task follows Devlin et al. (2018). Specifically, we select as supervision 15% of tokens randomly sampled from the sequence. For those 15% of tokens, we change the input token to a special "masking" token with 80% probability, a randomly-chosen alternate amino acid token with 10% probability, and the original input token (i.e. no change) with 10% probability. We take the loss to be the whole batch average cross entropy loss between the model's predictions and the true token for these 15% of amino acid tokens. In contrast to Devlin et al. (2018), we do not use any additional auxiliary prediction losses. The UniParc development models used in visualizations and in the supplemental results are trained with the masking procedure above. The UniRef models used across the experiments of the main text are trained similarly, except that for the 15% of tokens selected as prediction targets, all are replaced by the mask token.

Pre-training details Our model was pre-trained using a context size of 1024 tokens. As most Uniparc sequences (96.7%) contain fewer than 1024 amino acids, the Transformer is able to model the entire context in a single model pass. For those sequences that are longer than 1024 tokens, we sampled a random crop of 1024 tokens during each training epoch. The model was optimized using Adam ($\beta_1 = 0.9, \beta_2 = 0.999$) with learning rate 10^{-4}. We trained with 131,072 tokens per batch (128 gpus x 1024 tokens). The models follow a warm-up period of 16000 updates, during which the learning rate increases linearly. Afterwards, the learning rate follows an inverse square root decay schedule. All models were trained using the fairseq toolkit (Ott et al., 2019) on 128 NVIDIA V100 GPUs.

7. Evaluating the models for downstream tasks

After pre-training the model with unsupervised learning, we can adapt the parameters to supervised tasks. By passing the input sequence $(x_1, \ldots, x_n)$ through our pre-trained model, we obtain a final vector representation of the input sequence $(h_1, \ldots, h_n)$. During pre-training, this representation is projected to log probabilities $(y_1, \ldots, y_n)$. Recall that a softmax over y_i represents the model's posterior for the amino acid at position i. These final representations $(h_1, \ldots, h_n)$ are used directly, or fine-tuned in a task-dependent way by adding additional layers to the model and allowing the gradients to backpropagate through the weights of the pre-trained model to adapt them to the new task.

8. Language Modeling Baselines

In addition to comparing to past work, we also implemented deep learning baselines for our experiments.

Frequency (n-gram) models To establish a meaningful performance baseline on the sequence modeling task (Section 3), we construct n-gram frequency-based models for context sizes $1 \leq n \leq 10^4$, applying optimal Laplace smoothing for each context size. The Laplace smoothing hyperparameter in each case was tuned on the validation set. ECE is reported for the best left-conditioning n-gram model.

Bidirectional LSTM language models We trained state-of-the-art LSTM (Hochreiter & Schmidhuber, 1997) language models on the UR50 dataset. We use the ELMo model of Peters et al. (2018) which concatenates two independent autoregressive language models with left-to-right and right-to-left factorization. In contrast to standard LSTM models, the ELMo model receives context in both direction and is therefore comparable to the Transformers we train that also use the whole context of the sequence. We train two models: (i) the small model has approximately 28.4M parameters across 3 layers, with an embedding dimension of 512 and a hidden dimension of 1024; (ii) the large model has approximately 113.4M parameters across 3 layers, with an embedding dimension of 512 and a hidden dimension of 4096. The models are trained with a nominal batch size of 32,768, with truncated backpropagation to 100 tokens, dropout of 0.1, learning rate of 8e-4, using the Adam optimizer with betas of (0.9, 0.999), clip norm 0.1 and warmup of 1500 updates using an inverse square root learning rate schedule. We searched across a range of learning rates and found 8e-4 to be optimal.

Ablations on Transformer model To investigate the effect of pre-training, we compared to a Transformer with random weights (i.e. using the same random initializations as the pre-trained models, but without performing any pre-training). We refer to these baselines as "no pre-training", and elsewhere, we refer to these baselines as "untrained". Separately, to assess the effect of full network fine-tuning, we tested Transformer models where all weights outside task-specific layers are frozen during fine-tuning for the analysis. In these "projected" baselines, none of the base Transformer parameters are modified during fine-tuning.

9. Metric structure experiments

Full orthology dataset. For the analyses in Section 4, an orthologous group dataset was constructed from eggNOG 5.0 (Huerta-Cepas et al., 2018) by selecting 25 COG orthologous groups toward maximizing the size of the intersected set of species within each orthologous group. Through a greedy algorithm, we selected 25 COG groups with an intersecting set of 2609 species.

Diverse orthology dataset. For the analyses in Section 4 besides the aforementioned phylogenetic organization analysis, we shrank the dataset above by selecting only one species from each of 24 phyla in order to ensure species-level diversity.

10. Remote Homology

SCOP Dataset. We used the database of SCOP 2.07e filtered to 40% sequence similarity, provided by the ASTRAL compendium (Fox et al., 2014). Following standard practices (Steinegger et al., 2019), we exclude folds that are known to be related, specifically Rossman-like folds (c.2-c.5, c.27 and 28, c.30 and 31) and four- to eight-bladed β-propellers (b.66-b.70). This yields 256,806 pairs of remote homologs at the fold level and 92,944 at the superfamily level, consisting of 217 unique folds and 366 unique superfamilies. We then perform an 80-20 split, and tune our hyperparameters on the "training set" and report results on the held out 20% of the data. We refer to this dataset as SCOP40.

Metrics. Given a protein sequence s, with final hidden representation $(h_1, \ldots, h_n)$, we define the embedding of the sequence to be a vector e which is the average of the hidden representations across the positions in the sequence:

$$e = \frac{1}{n} \sum_{i=1}^{n} h_i$$

We can compare the similarity of two protein sequences, s and s' having embeddings e and e' using a metric in the embedding space.

We evaluate the L2 distance $\|e - e'\|_2$ and the cosine distance $e \cdot e' / \|e\| \|e'\|$. Additionally we evaluated the L2 distance after projecting the e vectors to the unit sphere.

Evaluation. To evaluate HHblits (Remmert et al., 2011), first we construct HMM profiles for each sequence using default parameters for 'hhblits', except we use 3 iterations. Then, we do an all-to-all alignment using 'hhalign' with default parameters, and use the resulting E-value as a measure of similarity. Given a query sequence, a sequence is more similar with a smaller E-value.

The two metrics reported are Hit-10 as introduced in Hou et al. (2018) and AUC. For both metrics, for each sequence, we treat it as a query and we rank each other sequence according to the distance metric used. Following Ma et al. (2014), when considering the fold level, we exclude all sequences that are similar at the superfamily level. Similarly, when considering the superfamily level, we exclude all sequences that are similar at the family level. This ensures we specifically measure how well our models do on finding *remote* homologs.

For Hit-10, we consider it a success if any of the top 10 sequences is a remote homolog. We report the proportion of successes averaged across all queries. For AUC, we first compute the AUC under the ROC curve when classifying sequences by vector similarity to the query. Then, we average the AUC across all query sequences.

We found that cosine similarity results in the best Hit-10 scores, while the L2 with unnormalized vectors result in the best AUC scores, so we report this in Table 2.

Implementation We used the FAISS similarity search engine (Johnson et al., 2017).

11. Representational similarity-based alignment of sequences within MSA families

Family selection For the analysis in Section 4, we selected structural families from the Pfam database (Bateman et al., 2013). We first filtered out any families whose longest sequence is less than 32 residues or greater than 1024 residues in length. We then ranked the families by the number of sequences contained in each family and selected the 128 largest families and associated MSAs. Finally, we reduced the size of each family to 128 sequences by uniform random sampling.

Aligned pair distribution For each family, we construct an empirical distribution of aligned residue pairs by enumerating all pairs of positions and indices that are aligned within the MSA and uniformly sampling 50000 pairs.

Unaligned pair distribution We also construct for each family a background empirical distribution of unaligned residue pairs. This background distribution needs to control for within-sequence position, since the residues of two sequences that have been aligned in an MSA are likely to occupy similar positions within their respective unaligned source sequences. Without controlling for this bias, a difference in the distributions of aligned and unaligned pairs could arise from representations encoding positional information rather than actual context. We control for this effect by sampling from the unaligned-pair distribution in proportion to the observed positional differences from the aligned-pair distribution. Specifically, the following process is repeated for each pair in the empirical aligned distribution:

1. Calculate the absolute value of the difference of each residue's within-sequence positions in the aligned pair.
2. Select a pair of sequences at random.
3. For that pair of sequences, select a pair of residues at random whose absolute value of positional difference equals the one calculated above.
4. Verify that the residues are unaligned in the MSA; if so, add the pair to the empirical background distribution.
5. Otherwise, return to step 2.

This procedure suffices to compute a empirical background distribution of 50000 unaligned residue pairs.

Similarity distributions Finally, for each family and each distribution, we apply the cosine similarity operator to each pair of residues to obtain the per-family aligned and unaligned distribution of representational cosine similarities.

12. Secondary structure experiments

12.1. Linear Projections

Evaluation For the analysis in Section 5.1, we derived and evaluated optimal linear projections of the representation of each position as follows. The linear projections were fit via multiclass logistic regression from the representation vectors to the secondary structure labels, with residues aggregated across all sequences in the training dataset.

We used an established secondary structure training dataset from Zhou & Troyanskaya (2014). The authors obtained a set of structures with better than 2.5Å resolution, with no two proteins having sequence similarity above 30%. The training set was further filtered to remove sequences with greater than 25% identity with the CB513 dataset (Cuff & Barton, 1999). This training dataset, labeled `5926_filtered` by the authors, contains the amino acid identities, Q8 (8-class) secondary structure labels, family-level frequency profiles, and miscellaneous other attributes for 5365 protein sequences.

For the test dataset, we used the CB513 dataset (Cuff & Barton, 1999), also as preprocessed by Zhou & Troyanskaya (2014). The only inputs that were provided to the network were raw sequences, and the outputs regressed were Q3 and Q8 secondary structure labels.

Single-family data and analysis For each of the three domains used, we extracted all domain sequences from the Pfam dataset (Bateman et al., 2013) and located the subset of PDB files containing the domain, using the latter to derive ground truth secondary structure labels (Kabsch & Sander, 1983).

Pre-training follows the methodology of Section 9 except that the datasets were from the domain sequences rather than UniParc sequences. The domain sequences were randomly partitioned into training, validation, and testing datasets. For each family, the training dataset comprises 65536 sequences, the validation dataset comprises either 16384 sequences

(PF00005 and PF00069) or 8192 sequences (PF00072), and the test dataset comprises the remainder.

Each Pfam family also forms an evaluation dataset for linear projection; from the sequences with corresponding crystal structures, the training dataset comprises 80 sequences and the test dataset comprises the remainder.

12.2. Deep neural networks and feature combination

We fine-tuned models trained on UR100, UR50/S, and UR50/D data derived from UniRef dated March 2018. We removed the final embedding layer, added layer norm, and applied a top-level architecture following (Klausen et al., 2019). In particular, this top-level architecture consists of two parallel convolution layers and an identity layer, whose outputs are concatenated in the feature dimension and fed to a two layer bidirectional LSTM containing 1024 hidden units and dropout $p = 0.5$. The output is then projected to an 8-dimensional feature vector at each position and the model is trained with a categorical cross-entropy loss with the Q8 data. The training data was obtained from the (Klausen et al., 2019). Secondary structure labels for the CASP13 test set were constructed using DSSP.

In feature combination experiments, we used the features provided by (Klausen et al., 2019) which were generated using MMseqs2 on the Uniclust90 dataset released April 2017. For CASP13 experiments, we generated these features using the code provided by (Klausen et al., 2019) on CASP13 domains.

As a baseline, we reimplemented (Klausen et al., 2019) by replacing the Transformer features with the MMseqs2 features and keeping the top-level architecture. For feature combination experiments, we projected (a) the features from this baseline and (b) the features from the Transformer to the same dimension (512 units), concatenated along the feature dimension, and fed the resulting tensor to a two layer bidirectional LSTM with 512 hidden units and dropout $p = 0.3$.

To check our dataset construction, we used the pretrained weights provided by (Klausen et al., 2019) and evaluated their model directly in our evaluation pipeline. We were able to reproduce the values reported in (Klausen et al., 2019).

13. Contact prediction experiments

13.1. Linear Projections

CATH Dataset For the analysis in Section 5.2, the dataset was derived from the S40 non-redundant set of domains in CATH (Orengo et al., 1997). The S40 subset has only those domain sequences where any pair of domains shares $< 40\%$ sequence identity. The contacts and sequences for each domain were extracted using the PDB files provided by CATH. The total number of files in this subset is $30,744$. Contacts were extracted following a standard criterion used in the literature (Jones et al., 2011), where a contact is defined as any pair of residues where the C$-\beta$ to C$-\beta$ distance (C$-\alpha$ to C$-\alpha$ distance in the case of glycine) is < 8 Å, and the residues are separated by at least 4 amino-acids in the original sequence.

We split non-contiguous protein chains into contiguous subsequences, and then filtered out sequences with less than 50 residues or more than 768 residues. This resulted in $32,994$ total data points (pairs of sequences and contact maps). We constructed train, validation, and test sets using these data points. We ensured that for each CATH domain which resulted in multiple contiguous subsequences, all the subsequences were confined to a single set (either train, valid or test). First, we randomly sampled a 10% subset of all sequences to obtain a test set. This resulted in 3339 test examples. The remaining sequences not assigned to test were filtered for similarity to the test sequences to produce the train and validation examples. All sequences that are similar to any sequence assigned to the test set were removed from the train and validation partition. To identify similar sequences, we used BLAST with an e-value of 0.1 and maximum sequence identity threshold of 20%. Using this filtering criteria, we ended up with $18,696$ remaining data points, which were randomly split into train and validation sets in the ratio $9:1$. This resulted in $16,796$ train $1,900$ validation examples.

To construct the 10% subset of the full fine-tuning dataset, we randomly sampled 10% of the train sequences to derive a smaller training set which had $1,557$ examples. The validation and test sets for the 10% training dataset are the same as used for the complete contact training dataset.

Projection method We add two linear projections, P and Q, with respective bias p and q to the final representations of the model:

$$y_{ij} = (Ph_i + p)^T (Qh_j + q)$$

These output y_{ij} the model's log probability of a contact between position i and position j that is fit with the binary cross entropy loss to the empirical contact map of the protein. Each projection is into 256 dimensions. We found re-scaling the predicted tensor by $1/256$ to be helpful in achieving higher accuracy.

13.2. Additional experiments with CATH dataset

The development Transformer models pre-trained on UniParc are evaluated for both linear projection and fine-tuning on the CATH dataset, in a full-data and low-data regime. Models are compared with and without pre-training. An

improvement in the ROC curve is seen to result from pre-training for both linear projections and fine-tuning.

We compare to convolutional neural network baselines where we embed the amino acids to a representation of dimension k, resulting in a k x N image (where N is the sequence length). We then apply a convolutional layer with C filters and kernel size M followed by a multilayer perceptron with hidden size D. We try different values of k, C, M and D, to get best performing models. The models are trained using Adam with $\beta_1 = 0.9, \beta_2 = 0.999$ and fixed learning rate $= 10^{-4}$.

13.3. Deep neural networks and feature combination

Data For the contact prediction results of Sections 4 and 5, we used the datasets and features distributed with Wang et al. (2017) and Xu (2018). The base features are those used by RaptorX (Xu, 2018) a state-of-the-art method in CASP13, including sequence features, PSSM, 3-state secondary structure prediction, predicted accessibility, one-hot embedding of sequence, and pairwise features APC-corrected Potts model couplings, mutual information, pairwise contact potential.

We use the training, standard test set, and CASP11 test set from Wang et al. (2017). We use the CASP12 test set from Xu (2018). For the CASP13 test set we use the 34 publicly released domains.

Wang et al. (2017) established training and test sets as follows. The train (6367 proteins), valid (400 proteins) and test (500 proteins) datasets were selected as subsets of PDB25 (each protein having <25% sequence similarity). Proteins having sequence similarity >25% or BLAST E-value <0.1 with any test or CASP11 protein were excluded from training data.

All our MSAs (used for the avg and cov combination methods) are constructed by running HHblits (Remmert et al., 2011) with 3 iterations and E-value 0.001 against Uniprot20 released on 2016-02; except for CASP12 and CASP13 where we used the four different MSAs released with and described in Xu (2018). Note that for the Transformer pre-training UniRef50 from 2018-03 was used; hence no data which was not already available prior to the start of CASP13 was present during either pre-training or contact prediction training.

Model architecture On top of the sequence and pairwise features we use a depth-32 residual network (ResNet) model to predict binary contacts. The ResNet model architecture is similar to Wang et al. (2017) and Xu (2018).

The first component of the ResNet is a learned sequence pipeline $y = f_\theta^S(x)$ which maps sequence features $x \in \mathbb{R}^{L \times d_1}$ to $y \in \mathbb{R}^{L \times d_2}$ with L the length of the protein. Though f_θ^S could be a 1D convolutional network or residual network as in Wang et al. (2017), we chose our sequence net to be a simple linear projection from input dimension d_1 to $d_2 = 128$ dimensions. The input dimension d_1 is either 46 (RaptorX only), 1280 (Transformer hidden state), or 1326 (feature combination). We varied d_1 and empirically determined 128 to be optimal.

The 128-D output y of the sequence net gets converted to pairwise matrix features z_1 with 256 feature maps, by the usual "outer concat" operation; i.e. at position i, j we concatenate y_i and y_j along the feature dimension, giving rise to $2 \times d_2$ feature maps. This $z_1 \in \mathbb{R}^{2d_2 \times L \times L}$ is then concatenated in the first (feature map or channel) dimension, with the pairwise features $z_2 \in \mathbb{R}^{6 \times L \times L}$ i.e. the pairwise RaptorX features described in previous subsection and/or the msa embedding covariance features ($z_3 \in \mathbb{R}^{256 \times L \times L}$) described in the next subsection. As such the concatenated $z \in \mathbb{R}^{262 \times L \times L}$ or $z \in \mathbb{R}^{518 \times L \times L}$.

The final component is the actual 2D residual network operating in z, which computes the binary contact probability $\hat{p} = g_\theta^R(z)$ with $\hat{p} \in \mathbb{R}^{L \times L}$ and $\hat{p}_{ij}$ the continuous predicted probability of position i and j of the protein being in contact. The ResNet has an initial 1×1 convolutional layer going to $d_3 = 128$ feature maps, followed by MaxOut over the feature maps with stride 2, reducing to 64 feature maps. After this, there are 32 residual blocks. Each residual block has on its weight path consecutively BatchNorm - ReLU - Conv 3×3 (64 feature maps) - Dropout (0.3) - ReLU - Conv 3×3 (64 feature maps). The residual blocks have consecutive dilation rates of 1,2,4. This follows Adhikari (2019). The final output is computed with a Conv 3×3 (1 output feature map) and sigmoid to produce probability of contact $\hat{p}_{ij} \in [0, 1]$. As such there are 66 convolutional layers in the main 2D ResNet.

Note that a number of shortcomings exist from our pipeline to CASP13 winners (Senior et al., 2018; Xu, 2018); most importantly we use an earlier training dataset of PDB structures compiled from PDB dated Feb 2015 by Wang et al. (2017), additionally we do not incorporate more recent developments like distance distribution prediction, sliding window on small crops allowing deeper ResNets, auxiliary losses like torsion angles, or data augmentation.

For reference, the officially released AlphaFold (Senior et al., 2018) predictions achieve a top-L/5,LR and top-L,LR precision on the same subset of CASP-13 targets of 75.2% and 52.2% respectively. The discrepancies in the pipeline explain why our best precisions using RaptorX features are about 7-9% lower (compare CASP13-AVG (a): 68.0% / 43.4%)

MSA Embedding feature combination. For the feature combination results in Section 6, we construct features

based on the embedding of the MSA of a protein sequence in our training data. We denote the original protein in our labeled dataset, i.e. query sequence s of length L, to have corresponding embedding $h = \text{Transformer}(s) \in \mathbb{R}^{L\times d}$, and the embedding of the i-th position to be $h_i \in \mathbb{R}^d$. Typically h is the last hidden state from the pre-trained Transformer model. The mth sequence in the MSA is s^m, with corresponding embedding h^m. $m \in [0, M[$ with M the MSA depth. The embeddings are computed by embedding the original sequence s^m without inserting gaps (there is no gap character in our vocabulary), then realigning the embedding according to the alignment between s^m and query sequence s by inserting 0-vectors at position i if the s_i^m is the gap character; ie $h_{i,k}^m = 0$. We also use indicator variable $\alpha_i^m = 1$ if s_i^m is non-gap (match state), or $\alpha_i^m = 0$ if s_i^m is gap. We further compute sequence weights w^m as the commonly used debiasing heuristic to reduce the influence of the oversampling of many similar sequences. The weights are defined in the usual way with 70% sequence similarity threshold: sequence weight $w^m = 1/|\{s^{m'}|seqid(s^m, s^{m'}) > 70\%\}|$ which is the inverse of the number of sequences $s^{m'}$ that are more than 70% similar to the sequence s^m i.e. hamming distance less than 0.3L.

Now we introduce the average embedding over an MSA, labeled "avg" in Section 6:

$$h_{ik}^{\text{avg}} = \frac{1}{M_{\text{eff}}(i)} \sum_{m=0}^{M-1} w^m \alpha_i^m h_{i,k}^m$$

with per-position denominator $M_{\text{eff}}(i) = \sum_{m=0}^{M-1} w^m \alpha_i^m$ This is effectively a weighted average over the sequence embeddings in the MSA. Note that if the embeddings were one-hot encodings of AA identities, we would recover the position probability matrix (except the absence of a pseudocount).

Similarly; we introduce the (uncentered) covariance of the embeddings, labeled "cov" in Section 6 with PCA-projected $\bar{h}$:

$$C_{ijkl} = \frac{1}{M_{\text{eff}}(i,j)} \sum_{m=0}^{M-1} w^m \alpha_i^m \bar{h}_{i,k}^m \alpha_j^m \bar{h}_{j,l}^m$$

With pairwise position denominator $M_{\text{eff}}(i,j) = \sum_{m=0}^{M-1} w^m \alpha_i^m \alpha_j^m$.

Note that to make above covariance embedding feasible, we first reduce the dimensionality of the embeddings by projecting onto the first 16 PCA directions: $\bar{h}_i = P h_i$ with $P \in \mathbb{R}^{16\times d}$, giving rise to a covariance per pair of positions i, j and pair of interacting PCA components k, l of $L \times L \times 16 \times 16$. The 256 different k, l pairs of $C_{ijkl} \in \mathbb{R}^{L\times L\times 16\times 16}$ will now become the feature maps of $z \in \mathbb{R}^{256\times L\times L}$, such that $z_{16k+l,i,j} = C_{ijkl}$. We tried training (rather than fixed PCA) the projection of the features $h \to \bar{h}$ before covariance (learned linear projection P or training a 3-layer MLP). We also varied the formulation to center the embeddings over the MSA (normal covariance) and to rescale the feature maps with a pre-computed mean and standard deviation for each feature map corresponding to a pair of k, l. We found no gains from these variations over the current formulation. Note that centering with the average h^{avg} as in normal empirical covariance calculation, introduces a shift that is independent per protein (because specific to the MSA), and independent per position. Therefore it is not unexpected that the uncentered covariance gives better (more consistent) features.

14. Mutagenesis Experiments in Section 7

Mutagenesis data For the analysis in Section 7, we used two datasets of variant effect measurements compiled by Gray et al. (2018) and Riesselman et al. (2018). The first dataset is a collection of 21,026 measurements from nine experimental deep mutational scans. The second dataset contains 712,218 mutations across 42 deep mutational scans.

Fine-tuning procedure To fine-tune the model to predict the effect of changing a single amino acid or combination of amino acids we regress the scaled mutational effect with:

$$y = \sum_i \log p_i(\text{mt}(i)) - \log p_i(\text{wt}(i))$$

Where $\text{mt}(i)$ is the mutated amino acid at position i, and $\text{wt}(i)$ is the wildtype amino acid. The sum runs over the indices of the mutated positions. As an evaluation metric, we report the Spearman ρ between the model's predictions and experimentally measured values.

15. Additional

Area under the ROC curve Area under the ROC curve measures the performance on a classification problem at various threshold settings. ROC is a probability curve illustrating the relationship between the true positive rate and false positive rate for a binary classification task, and AUC represents degree or measure of separability. It quantifies the model's capability of distinguishing between classes. Intuitively a perfect classifier has an AUC of 1, while a uniform random classifier has an AUC of 0.5.

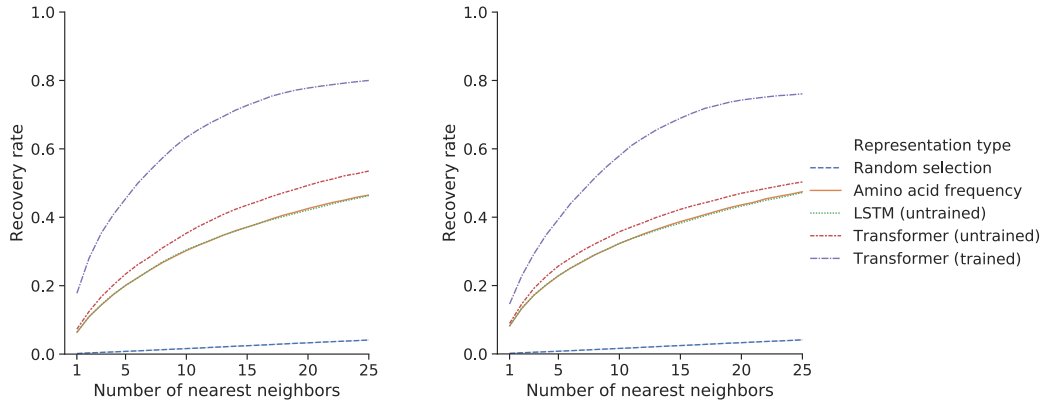

(a) Recovery rates under group translation

(b) Recovery rate under species translation

Figure S1. Learned sequence representations can be translated between orthologous groups and species. Depicted is the recovery rate of nearest-neighbor search under (a) orthologous group translation, and (b) species translation; in both settings, the trained Transformer representation space has a higher recovery rate. Results shown for 36-layer dev Transformer pre-trained on UniParc. To define a linear translation between protein a and protein b of the same species, we define the source and target sets as the average of protein a or protein b across all 24 diverse species. If representation space linearly encodes orthology, then adding the difference in these averages to protein a of some species will recover protein b in the same species. We use an analogous approach to translate a protein of a source species s to its ortholog in the target species t. Here, we consider the average representation of the proteins in s and in t. If representation space is organized linearly by species, then adding the difference in average representations to a protein in species s will recover the corresponding protein in species t.

Representation type	Overall	Identical amino acid pairs	Distinct amino acid pairs
Transformer (trained)	**0.841**	**0.870**	**0.792**
Transformer (untrained)	0.656	0.588	0.468

Table S3. Area under the ROC curve (AUC) of per-residue representational cosine similarities in distinguishing between aligned and unaligned pairs of residues within a Pfam family. Results displayed are averaged across 128 families.

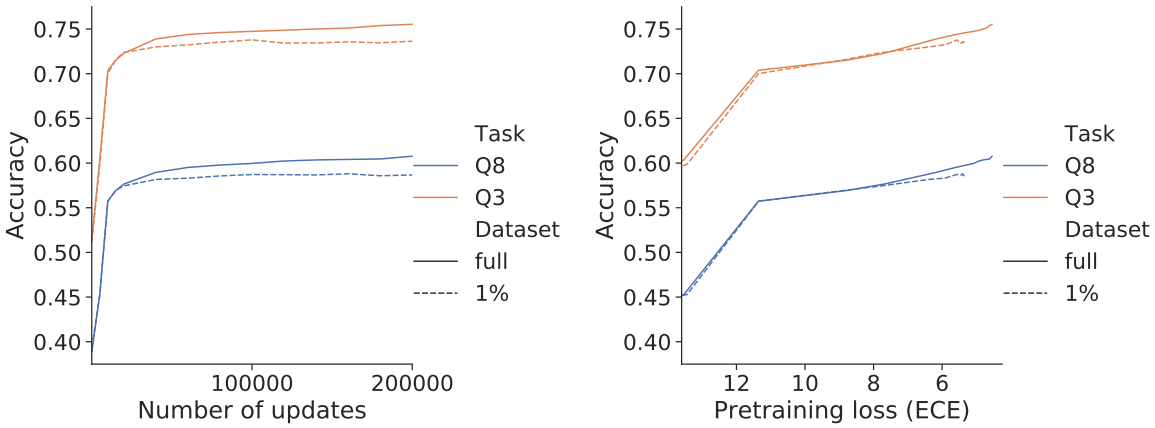

Figure S2. Linearly recoverable information about secondary structure increases rapidly in the early phases of training and shows an inverse relationship with the model's ECE. Top-1 secondary structure prediction test accuracy for linear projections of the final hidden representations are reported. Models are trained on the full UniParc dataset and a random subsample of 1% of the UniParc dataset. Left panel depicts accuracy as a function of model pre-training update steps. Right panel depicts accuracy as a function of pre-training loss. Results shown for 36-layer dev Transformer pre-trained on UniParc.

Representation type	Q8		Q3	
	Train (cullpdb)	**Test (CB513)**	**Train (cullpdb)**	**Test (CB513)**
Amino acid identity (prior)	0.375	0.348	0.490	0.488
PSSM	0.453	0.421	0.577	0.566
PSSM + amino acid identity	0.454	0.422	0.577	0.566
12-layer Transformer (untrained)	0.420	0.390	0.523	0.519
24-layer Transformer (untrained)	0.418	0.393	0.521	0.520
36-layer Transformer (untrained)	0.417	0.388	0.519	0.515
12-layer Transformer (Uniparc full)	0.624	0.581	0.752	0.731
24-layer Transformer (Uniparc full)	0.636	0.592	0.765	0.740
36-layer Transformer (Uniparc 1%)	0.632	0.587	0.760	0.737
36-layer Transformer (Uniparc full)	**0.655**	**0.608**	**0.782**	**0.755**

Table S4. Linear recovery of secondary structure information. Top-1 secondary structure prediction accuracy is reported for an optimal linear projection of per-residue representations on the dataset from Zhou & Troyanskaya (2014). For Transformer models, the pre-training dataset is stated in parentheses. Q8 denotes 8-class prediction task, Q3 denotes 3-class prediction task.

Model type	Full CATH data	10% CATH data
Transformer (pre-trained, fine-tuned)	0.863	0.806
Transformer (pre-trained, projected)	0.842	0.810
Transformer (no pre-training, fine-tuned)	0.783	0.727
Transformer (no pre-training, projected)	0.739	0.732
Convolutional	0.764	0.724

Table S5. Average AUC values on CATH domain test set. Linear projections of pre-trained representations recover residue-residue contacts. A significant gain in recovery is observed as a result of pre-training. Supervised fine-tuning of the weights of the Transformer model increases recovery. Additionally unsupervised pre-training enables generalization of residue-residue contact information from a small fraction of the training examples. Results are shown comparing supervision from the full CATH training set with 10% of the training data. ROC curves are shown in Figure S3. Pre-trained models combined with 10% of the contact data outperform models without pre-training that use 100% of the data. Results shown for 36-layer dev Transformer pre-trained on UniParc.

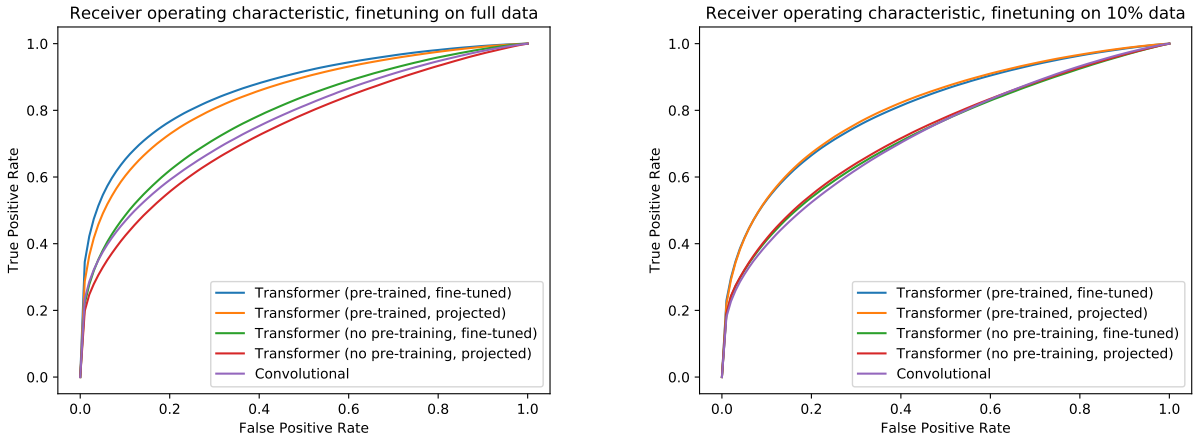

(a) (b)

Figure S3. Average ROC curves for the pre-trained Transformer model and comparison models supervised using (a) the full CATH training dataset, and (b) 10% of the CATH training dataset. The ROC curves for each model are averaged over all test dataset sequences. Results shown for 36-layer dev Transformer pre-trained on UniParc.

Metric: top-		L/5,LR	L,LR	L/5,MR	L,MR	L/5,SR	L,SR
Test	(a) RaptorX	84.3 ± .2	59.4 ± .2	74.4 ± .1	33.0 ± .0	71.6 ± .1	25.8 ± .0
	(b) +direct	86.7 ± .3	61.7 ± .4	76.5 ± .3	33.8 ± .1	**73.6 ± .2**	**26.1 ± .1**
	(c) +avg	**87.7 ± .3**	62.9 ± .4	77.4 ± .2	**34.0 ± .1**	**73.7 ± .3**	**26.1 ± .1**
	(d) +cov	**87.8 ± .3**	**63.3 ± .2**	**77.6 ± .2**	**34.0 ± .1**	**73.7 ± .2**	**26.1 ± .0**
CASP11	(a) RaptorX	77.5 ± .4	53.8 ± .3	75.0 ± .5	35.6 ± .2	72.1 ± .6	28.6 ± .2
	(b) +direct	78.3 ± .1	55.0 ± .1	76.2 ± .4	35.9 ± .2	74.0 ± .5	28.8 ± .2
	(c) +avg	**80.4 ± .5**	56.6 ± .4	**76.5 ± .4**	36.3 ± .2	**73.8 ± .5**	28.8 ± .1
	(d) +cov	**80.3 ± .3**	**56.8 ± .2**	**76.6 ± .4**	**36.5 ± .2**	**74.0 ± .4**	**29.0 ± .0**
CASP12-AVG	(a) RaptorX	72.7 ± .6	51.1 ± .2	68.3 ± .5	31.2 ± .3	66.5 ± .2	26.3 ± .1
	(b) +direct	74.0 ± .8	51.5 ± .5	70.7 ± .7	**32.4 ± .3**	68.9 ± .9	**27.2 ± .2**
	(c) +avg	74.4 ± 1.4	52.4 ± .5	**71.7 ± .6**	**32.2 ± .3**	**70.1 ± .2**	26.9 ± .2
	(d) +cov	**76.6 ± .7**	**53.0 ± .3**	70.1 ± .3	31.9 ± .3	69.1 ± .5	26.6 ± .1
CASP12-ENS	(a) RaptorX	77.1 ± .9	54.5 ± .4	70.6 ± .6	32.4 ± .4	68.6 ± .4	27.0 ± .1
	(b) +direct	77.0 ± .6	53.5 ± .6	**71.9 ± .9**	**33.1 ± .3**	69.8 ± .7	**27.6 ± .2**
	(c) +avg	76.7 ± 1.4	54.4 ± .7	**74.1 ± .8**	**33.0 ± .3**	**71.5 ± .3**	27.4 ± .2
	(d) +cov	**79.7 ± .8**	**55.3 ± .2**	72.7 ± .5	32.7 ± .3	71.0 ± .6	27.2 ± .2
CASP13-AVG	(a) RaptorX	68.0 ± .9	43.4 ± .4	71.3 ± .4	36.5 ± .3	68.8 ± 1.0	28.4 ± .0
	(b) +direct	67.4 ± .8	43.7 ± .4	69.5 ± .9	35.5 ± .4	68.1 ± .4	28.3 ± .2
	(c) +avg	68.1 ± 1.6	**44.8 ± .8**	**73.0 ± .6**	**36.9 ± .1**	**71.2 ± .6**	**28.6 ± .2**
	(d) +cov	**70.3 ± 1.3**	**45.2 ± .5**	**73.5 ± 1.4**	**37.0 ± .2**	70.2 ± .8	**28.6 ± .3**
CASP13-ENS	(a) RaptorX	**72.1 ± .8**	46.3 ± .5	73.6 ± .4	**38.1 ± .3**	71.0 ± 1.4	**29.6 ± .1**
	(b) +direct	68.0 ± .7	45.0 ± .6	71.4 ± 1.2	36.6 ± .4	70.2 ± .2	29.1 ± .2
	(c) +avg	70.8 ± 2.2	46.4 ± 1.1	**75.4 ± .5**	**38.1 ± .2**	**73.6 ± .5**	29.3 ± .2
	(d) +cov	71.9 ± 1.9	**47.2 ± .4**	**75.2 ± 1.5**	**38.3 ± .4**	**72.3 ± .8**	29.3 ± .2

Table S6. Additional metrics on the same test sets and feature combinations as Table 7. AVG corresponds to the average of the metrics over the different MSAs, while in ENS the probabilities are averaged (ensembled) over the different MSA predictions before computing the metrics.

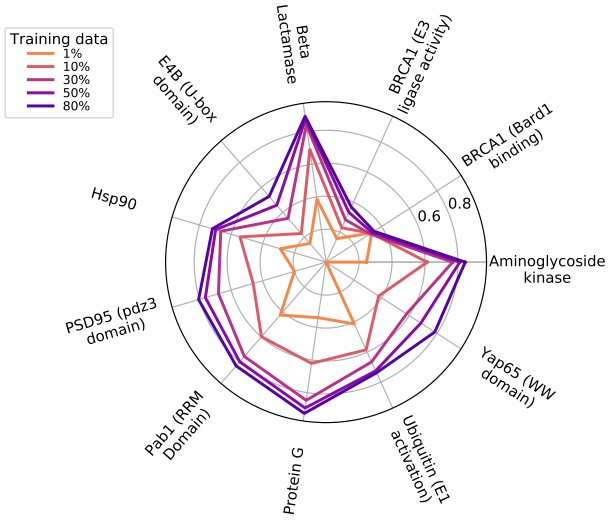

Figure S4. After pre-training, the Transformer can be adapted to predict mutational effects on protein function. The 34-layer Transformer model pre-trained on UR50/S is fine-tuned on mutagenesis data. Spearman ρ on each protein when supervised with smaller fractions of the data.

Amount of training data Protein	1% data	10% data	30% data	50% data	80% data
Aminoglycoside kinase	0.25 ± 0.07	0.61 ± 0.02	0.77 ± 0.01	0.81 ± 0.01	0.84 ± 0.01
BRCA1 (Bard1 binding)	0.33 ± 0.02	0.32 ± 0.01	0.32 ± 0.03	0.33 ± 0.03	0.35 ± 0.03
BRCA1 (E3 ligase activity)	0.16 ± 0.01	0.23 ± 0.03	0.28 ± 0.07	0.33 ± 0.05	0.37 ± 0.04
Beta Lactamase	0.39 ± 0.03	0.69 ± 0.01	0.84 ± 0.01	0.88 ± 0.01	0.89 ± 0.01
E4B (U-box domain)	0.15 ± 0.03	0.23 ± 0.03	0.35 ± 0.01	0.46 ± 0.03	0.53 ± 0.04
Hsp90	0.29 ± 0.02	0.54 ± 0.01	0.67 ± 0.01	0.70 ± 0.02	0.72 ± 0.05
PSD95 (pdz3 domain)	0.20 ± 0.02	0.46 ± 0.05	0.68 ± 0.01	0.76 ± 0.01	0.81 ± 0.02
Pab1 (RRM Domain)	0.42 ± 0.07	0.60 ± 0.02	0.76 ± 0.01	0.80 ± 0.01	0.83 ± 0.02
Protein G	0.34 ± 0.15	0.62 ± 0.03	0.85 ± 0.02	0.89 ± 0.02	0.93 ± 0.01
Ubiquitin (E1 activation)	0.41 ± 0.06	0.58 ± 0.02	0.67 ± 0.02	0.72 ± 0.02	0.74 ± 0.02
Yap65 (WW domain)		0.38 ± 0.06	0.58 ± 0.06	0.68 ± 0.05	0.78 ± 0.05

Table S7. Aggregate spearman ρ measured across models and datasets. Mean and standard deviations of spearman ρ performance for the fine-tuned Transformer-34 on intraprotein tasks. Performance was assessed on five random partitions of the validation set. Model pre-trained on UR50/S.

dataset model	spearmanr Envision	Envision (LOPO)	DeepSequence
Transformer	0.71 ± 0.20	0.51	0.70 ± 0.15
LSTM biLM (Large)	0.65 ± 0.22		0.62 ± 0.19
Gray, et al. 2018	0.64 ± 0.21	0.45	
Riesselman, et al. 2018			0.48 ± 0.26

Table S8. Aggregate spearman ρ measure across models and datasets. 34-layer Transformer pre-trained on UR50/S. For intraprotein models, the train/valid data was randomly partitioned five times. The mean $\pm$ standard deviation across the five runs is reported. No standard deviations are reported for LOPO experiments, as the evaluation is performed across all proteins.

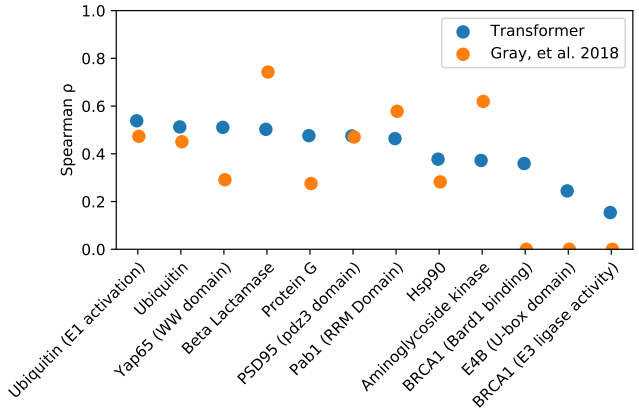

Figure S5. Leave-one-out experiment on Envision dataset (Gray et al., 2018). Pre-training improves the ability of the Transformer to generalize to the mutational fitness landscape of held-out proteins. All mutagenesis data from the protein selected for evaluation are held out, and the model is supervised with data from the remaining proteins. For each evaluation protein, a comparison is shown for the 34-layer Transformer pre-trained on UR50/S.

Model	Pre-Training	Params	SSP		Contact			
			CB513	CASP13	Test	CASP11	CASP12	CASP13
Transformer-34	(None)	669.2M	56.8	60.0	16.3	17.7	14.8	13.3
UniRep (LSTM)		18.2M	58.4	60.1	21.9	21.4	16.8	14.3
SeqVec (LSTM)		93M	62.1	64.0	29.0	25.5	23.6	17.9
TAPE (Transformer)		38M	58.0	61.5	23.2	23.8	20.3	16.0
LSTM biLM (S)	UR50/S	28.4M	60.4	63.2	24.1	23.6	19.9	15.3
LSTM biLM (L)	UR50/S	113.4M	62.4	64.1	27.8	26.4	24.0	16.4
Transformer-6	UR50/S	42.6M	62.0	64.2	30.2	29.9	25.3	19.8
Transformer-12	UR50/S	85.1M	65.4	67.2	37.7	33.6	27.8	20.7
Transformer-34	UR100	669.2M	64.3	66.5	32.7	28.9	24.3	19.1
Transformer-34	UR50/S	669.2M	**69.1**	**70.7**	**50.2**	**42.8**	**34.7**	**30.1**

Table S9. Comparison to related methods, extended version. Prediction from single sequence, no evolutionary features or MSA construction. Top-L long-range contact precision. Test is RaptorX test set of Wang et al. (2017). Model weights for related work are obtained and evaluated in our codebase with same downstream architecture, training, and test data.

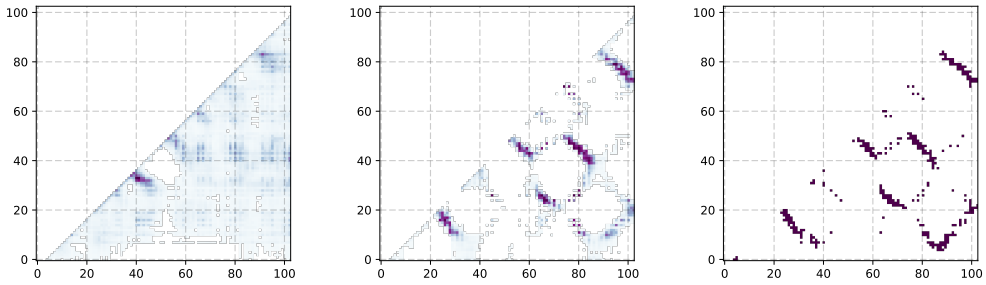

No pre-training, fine-tuned | Pre-trained, fine-tuned | True contacts 2edyA00 (1-104)

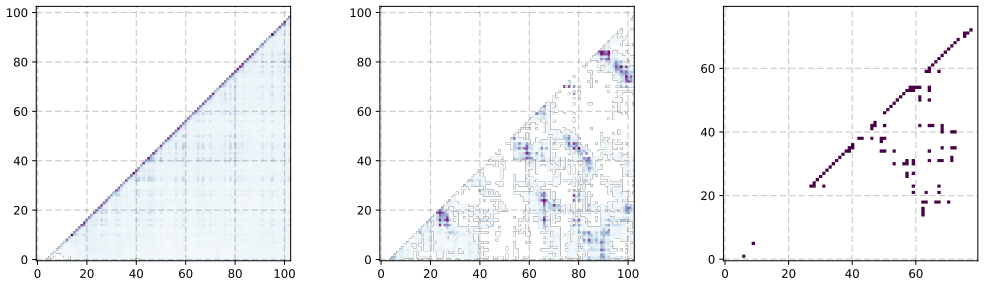

No pre-training, projected | Pre-trained, projected | Train NN, 1wh5A00 (1-81)

(a) 2edyA00 (1-104)

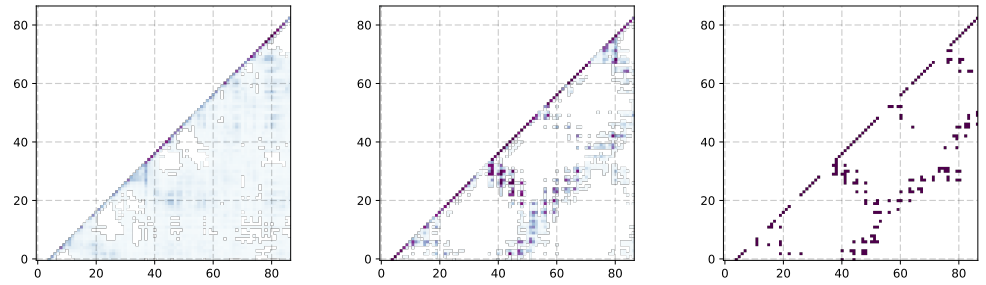

No pre-training, fine-tuned | Pre-trained, fine-tuned | True contacts 2iw3A01 (68-155)

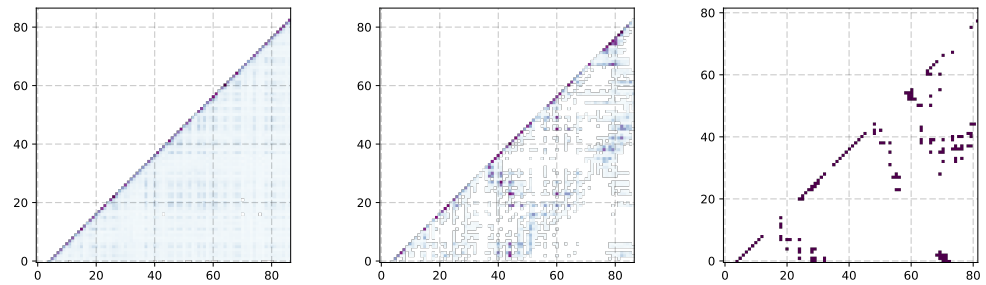

No pre-training, projected | Pre-trained, projected | Train NN, 2b7uA02 (170-252)

(b) 2iw3A01 (68-155)

Figure S6. Predictions for a selection of CATH domains in the test set with diverse folds. Predictions of the fine-tuned models are compared with and without pre-training, along with projections of the final hidden representations with and without pre-training. For each test sequence, the nearest neighbor by sequence identity in the training dataset is shown. Transformer models are able to generalize supervision from contacts and do not trivially copy the contact pattern of the nearest neighbor sequence. Visualizations from the 36-layer Transformer trained on UniParc.

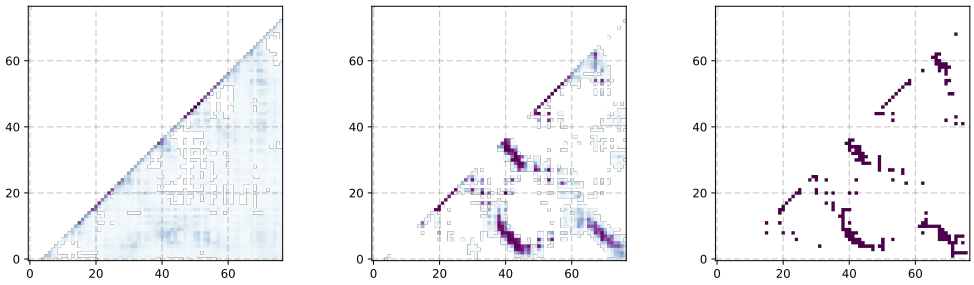

No pre-training, fine-tuned | Pre-trained, fine-tuned | True contacts 2jvoA00 (28-105)

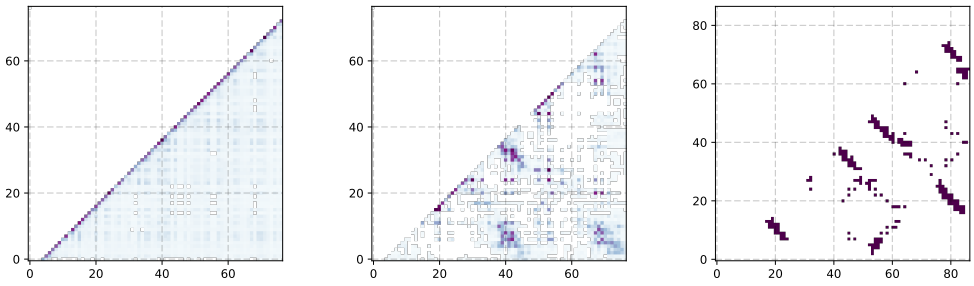

No pre-training, projected | Pre-trained, projected | Train NN, 4rzkA00 (78-165)

(c) 2jvoA00 (28-105)

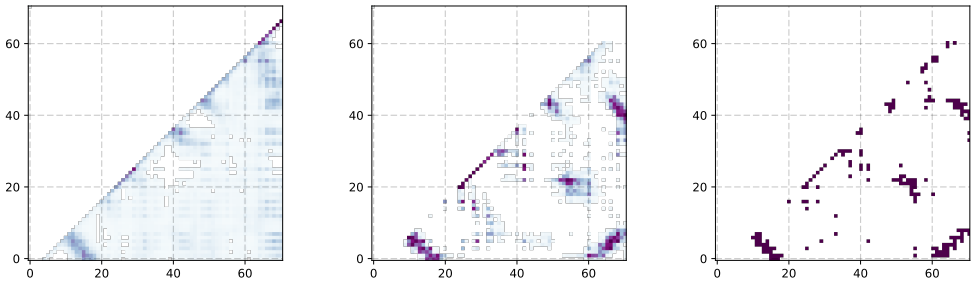

No pre-training, fine-tuned | Pre-trained, fine-tuned | True contacts 2kd0A01 (12-83)

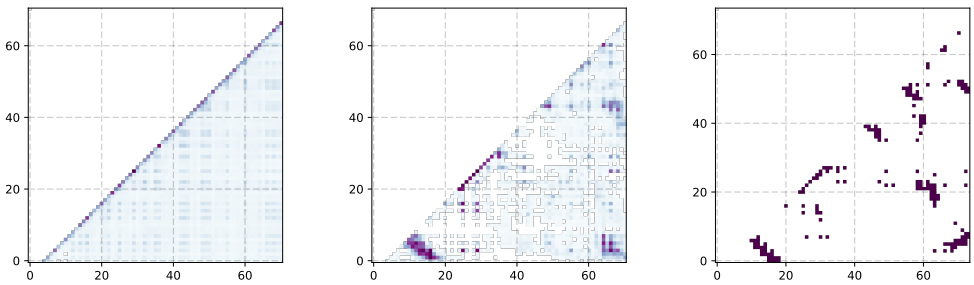

No pre-training, projected | Pre-trained, projected | Train NN, 1dgjA01 (1-75)

(d) 2kd0A01 (12-83)

Figure S6. continued from above.

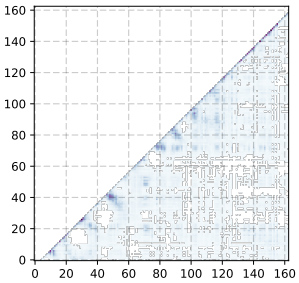

No pre-training, fine-tuned

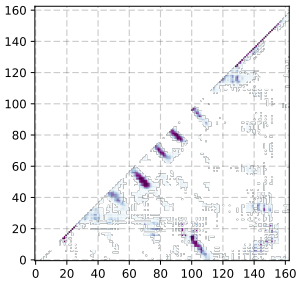

Pre-trained, fine-tuned

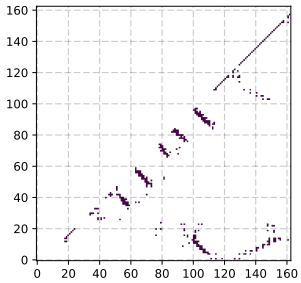

True contacts 2m47A00 (1-164)

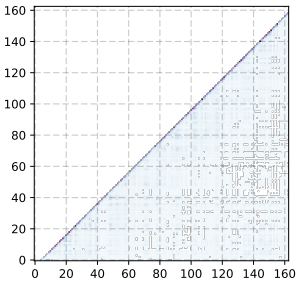

No pre-training, projected

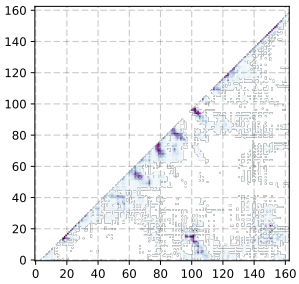

Pre-trained, projected

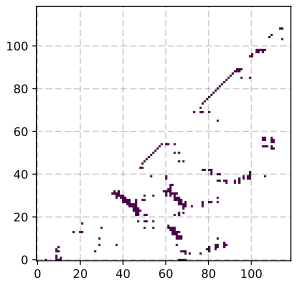

Train NN, 2lwfA00 (62-181)

(e) 2m47A00

Figure S6. continued from above.

Supplemental References

Adhikari, B. DEEPCON: protein contact prediction using dilated convolutional neural networks with dropout. *Bioinformatics*, 36(2):470–477, 07 2019.

Ba, J. L., Kiros, J. R., and Hinton, G. E. Layer normalization. *arXiv preprint arXiv:1607.06450*, 2016.

Balakrishnan, S., Kamisetty, H., Carbonell, J. G., Lee, S.-I., and Langmead, C. J. Learning generative models for protein fold families. *Proteins: Structure, Function, and Bioinformatics*, 79(4):1061–1078, 2011.

Bateman, A., Heger, A., Sonnhammer, E. L. L., Mistry, J., Clements, J., Tate, J., Hetherington, K., Holm, L., Punta, M., Coggill, P., Eberhardt, R. Y., Eddy, S. R., and Finn, R. D. Pfam: the protein families database. *Nucleic Acids Research*, 42(D1):D222–D230, 11 2013. ISSN 0305-1048. doi: 10.1093/nar/gkt1223.

Bengio, Y., Ducharme, R., Vincent, P., and Jauvin, C. A neural probabilistic language model. *Journal of machine learning research*, 3(Feb):1137–1155, 2003.

Chapelle, O., Schölkopf, B., and Zien, A. *Semi-Supervised Learning*. The MIT Press, 2006.

Cuff, J. A. and Barton, G. J. Evaluation and improvement of multiple sequence methods for protein secondary structure prediction. *Proteins: Structure, Function, and Bioinformatics*, 34(4):508–519, 1999.

Devlin, J., Chang, M., Lee, K., and Toutanova, K. BERT: pre-training of deep bidirectional transformers for language understanding. *CoRR*, abs/1810.04805, 2018. URL http://arxiv.org/abs/1810.04805.

Eddy, S. R. Profile hidden markov models. *Bioinformatics*, 14(9):755–763, 10 1998. ISSN 1367-4803. doi: 10.1093/bioinformatics/14.9.755.

Ekeberg, M., Lövkvist, C., Lan, Y., Weigt, M., and Aurell, E. Improved contact prediction in proteins: using pseudolikelihoods to infer potts models. *Physical Review E*, 87(1):012707, 2013.

Fox, N. K., Brenner, S. E., and Chandonia, J.-M. SCOPe: Structural Classification of Proteins—extended, integrating SCOP and ASTRAL data and classification of new structures. *Nucleic Acids Research*, 42(D1): D304–D309, January 2014. ISSN 0305-1048, 1362-4962. doi: 10.1093/nar/gkt1240. URL https://academic.oup.com/nar/article-lookup/doi/10.1093/nar/gkt1240.

Gray, V. E., Hause, R. J., Luebeck, J., Shendure, J., and Fowler, D. M. Quantitative missense variant effect prediction using large-scale mutagenesis data. *Cell systems*, 6(1):116–124, 2018.

He, K., Zhang, X., Ren, S., and Sun, J. Identity mappings in deep residual networks. In *European conference on computer vision*, pp. 630–645. Springer, 2016.

Hendrycks, D. and Gimpel, K. Gaussian error linear units (gelus). *arXiv preprint arXiv:1606.08415*, 2016.

Hinton, G. E. and Salakhutdinov, R. R. Reducing the dimensionality of data with neural networks. *science*, 313 (5786):504–507, 2006.

Hochreiter, S. and Schmidhuber, J. Long short-term memory. *Neural Computation*, 9(8):1735–1780, 1997. doi: 10.1162/neco.1997.9.8.1735.

Hochreiter, S., Bengio, Y., and Frasconi, P. Gradient flow in recurrent nets: the difficulty of learning long-term dependencies. 2001.

Hou, J., Adhikari, B., and Cheng, J. DeepSF: deep convolutional neural network for mapping protein sequences to folds. *Bioinformatics (Oxford, England)*, 34 (8):1295–1303, 2018. ISSN 1367-4811. doi: 10.1093/bioinformatics/btx780.

Huerta-Cepas, J., Forslund, S. K., Bork, P., Hernández-Plaza, A., von Mering, C., Szklarczyk, D., Heller, D., Cook, H., Jensen, L., Mende, D. R., Letunic, I., and Rattei, T. eggNOG 5.0: a hierarchical, functionally and phylogenetically annotated orthology resource based on 5090 organisms and 2502 viruses. *Nucleic Acids Research*, 47(D1):D309–D314, 11 2018. ISSN 0305-1048. doi: 10.1093/nar/gky1085.

Johnson, J., Douze, M., and Jégou, H. Billion-scale similarity search with gpus. *CoRR*, abs/1702.08734, 2017. URL http://arxiv.org/abs/1702.08734.

Jones, D. T., Buchan, D. W., Cozzetto, D., and Pontil, M. Psicov: precise structural contact prediction using sparse inverse covariance estimation on large multiple sequence alignments. *Bioinformatics*, 28(2):184–190, 2011.

Kabsch, W. and Sander, C. Dictionary of protein secondary structure: pattern recognition of hydrogen-bonded and geometrical features. *Biopolymers*, 22(12):2577–2637, 1983.

Khandelwal, U., He, H., Qi, P., and Jurafsky, D. Sharp nearby, fuzzy far away: How neural language models use context. In *Proceedings of the 56th Annual Meeting of the Association for Computational Linguistics (Volume 1: Long Papers)*, pp. 284–294, 2018.

Kihara, D. The effect of long-range interactions on the secondary structure formation of proteins. *Protein Sci*, 2005. doi: 10.1110/ps.051479505.

Klausen, M. S., Jespersen, M. C., Nielsen, H., Jensen, K. K., Jurtz, V. I., Sonderby, C. K., Sommer, M. O. A., Winther, O., Nielsen, M., Petersen, B., and Marcatili, P. NetSurfP-2.0: Improved prediction of protein structural features by integrated deep learning. *Proteins*, 87(6):520–527, 06 2019.

Kryshtafovych, A., Schwede, T., Topf, M., Fidelis, K., and Moult, J. Critical assessment of methods of protein structure prediction (casp)—round xiii. *Proteins: Structure, Function, and Bioinformatics*, 87(12):1011–1020, 2019.

Lample, G., Denoyer, L., and Ranzato, M. Unsupervised machine translation using monolingual corpora only. *CoRR*, abs/1711.00043, 2017. URL http://arxiv.org/abs/1711.00043.

Ma, J., Wang, S., Wang, Z., and Xu, J. Mrfalign: protein homology detection through alignment of markov random fields. In *International Conference on Research in Computational Molecular Biology*, pp. 173–174. Springer, 2014.

Marks, D. S., Colwell, L. J., Sheridan, R., Hopf, T. A., Pagnani, A., Zecchina, R., and Sander, C. Protein 3d structure computed from evolutionary sequence variation. *PloS one*, 6(12):e28766, 2011.

Mikolov, T., Chen, K., Corrado, G., and Dean, J. Efficient estimation of word representations in vector space. In *1st International Conference on Learning Representations, ICLR 2013, Scottsdale, Arizona, USA, May 2-4, 2013, Workshop Track Proceedings*, 2013a. URL http://arxiv.org/abs/1301.3781.

Mikolov, T., Sutskever, I., Chen, K., Corrado, G. S., and Dean, J. Distributed representations of words and phrases and their compositionality. In *Advances in neural information processing systems*, pp. 3111–3119, 2013b.

Mirdita, M., von den Driesch, L., Galiez, C., Martin, M. J., Söding, J., and Steinegger, M. Uniclust databases of clustered and deeply annotated protein sequences and alignments. *Nucleic acids research*, 45(D1):D170–D176, 2017.

Morcos, F., Pagnani, A., Lunt, B., Bertolino, A., Marks, D. S., Sander, C., Zecchina, R., Onuchic, J. N., Hwa, T., and Weigt, M. Direct-coupling analysis of residue coevolution captures native contacts across many protein families. *Proceedings of the National Academy of Sciences*, 108(49):E1293–E1301, 2011.

Moult, J., Fidelis, K., Kryshtafovych, A., Schwede, T., and Tramontano, A. Critical assessment of methods of protein structure prediction: Progress and new directions in round xi. *Proteins: Structure, Function, and Bioinformatics*, 84: 4–14, 2016.

Moult, J., Fidelis, K., Kryshtafovych, A., Schwede, T., and Tramontano, A. Critical assessment of methods of protein structure prediction (casp)—round xii. *Proteins: Structure, Function, and Bioinformatics*, 86:7–15, 2018.

Orengo, C. A., Michie, A., Jones, S., Jones, D. T., Swindells, M., and Thornton, J. M. Cath–a hierarchic classification of protein domain structures. *Structure*, 5(8):1093–1109, 1997.

Ott, M., Edunov, S., Baevski, A., Fan, A., Gross, S., Ng, N., Grangier, D., and Auli, M. fairseq: A fast, extensible toolkit for sequence modeling. In *Proceedings of NAACL-HLT 2019: Demonstrations*, 2019.

Pennington, J., Socher, R., and Manning, C. D. Glove: Global vectors for word representation. In *Proceedings of the 2014 Conference on Empirical Methods in Natural Language Processing, EMNLP 2014, October 25-29, 2014, Doha, Qatar, A meeting of SIGDAT, a Special Interest Group of the ACL*, pp. 1532–1543, 2014. URL http://aclweb.org/anthology/D/D14/D14-1162.pdf.

Peters, M. E., Neumann, M., Iyyer, M., Gardner, M., Clark, C., Lee, K., and Zettlemoyer, L. Deep contextualized word representations. In *Proceedings of the 2018 Conference of the North American Chapter of the Association for Computational Linguistics: Human Language Technologies, NAACL-HLT 2018, New Orleans, Louisiana, USA, June 1-6, 2018, Volume 1 (Long Papers)*, pp. 2227–2237, 2018. URL https://aclanthology.info/papers/N18-1202/n18-1202.

Radford, A., Narasimhan, K., Salimans, T., and Sutskever, I. Improving language understanding by generative pre-training. 2018.

Radford, A., Wu, J., Child, R., Luan, D., Amodei, D., and Sutskever, I. Language models are unsupervised multitask learners. 2019.

Remmert, M., Biegert, A., Hauser, A., and Söding, J. Hhblits: lightning-fast iterative protein sequence searching by hmm-hmm alignment. *Nature Methods*, 9:173 EP, 12 2011. doi: 10.1038/nmeth.1818.

Riesselman, A. J., Ingraham, J. B., and Marks, D. S. Deep generative models of genetic variation capture the effects of mutations. *Nature Methods*, 15(10):816–822, 2018. ISSN 1548-7105. doi: 10.1038/s41592-018-0138-4.

Senior, A., Jumper, J., and Hassabis, D. AlphaFold: Using AI for scientific discovery, 12 2018. URL https://deepmind.com/blog/alphafold/.

Söding, J. Protein homology detection by hmm–hmm comparison. *Bioinformatics*, 21(7):951–960, 2004.

Steinegger, M. and Söding, J. Mmseqs2 enables sensitive protein sequence searching for the analysis of massive data sets. *Nature biotechnology*, 35(11):1026–1028, 2017.

Steinegger, M., Meier, M., Mirdita, M., Vöhringer, H., Haunsberger, S. J., and Söding, J. HH-suite3 for fast remote homology detection and deep protein annotation. *BMC Bioinformatics*, 20(1):473, September 2019. ISSN 1471-2105. doi: 10.1186/s12859-019-3019-7. URL https://doi.org/10.1186/s12859-019-3019-7.

Sun, C., Myers, A., Vondrick, C., Murphy, K., and Schmid, C. Videobert: A joint model for video and language representation learning. *CoRR*, abs/1904.01766, 2019. URL http://arxiv.org/abs/1904.01766.

Suzek, B. E., Wang, Y., Huang, H., McGarvey, P. B., Wu, C. H., and Consortium, U. Uniref clusters: a comprehensive and scalable alternative for improving sequence similarity searches. *Bioinformatics*, 31(6):926–932, 2015.

The UniProt Consortium. The universal protein resource (uniprot). *Nucleic Acids Research*, 36(suppl_1):D190–D195, 11 2007. ISSN 0305-1048. doi: 10.1093/nar/gkm895.

Vaswani, A., Shazeer, N., Parmar, N., Uszkoreit, J., Jones, L., Gomez, A. N., Kaiser, Ł., and Polosukhin, I. Attention is all you need. In *Advances in neural information processing systems*, pp. 5998–6008, 2017.

Wang, S., Sun, S., Li, Z., Zhang, R., and Xu, J. Accurate de novo prediction of protein contact map by ultra-deep learning model. *PLoS computational biology*, 13(1): e1005324, 2017.

Weigt, M., White, R. A., Szurmant, H., Hoch, J. A., and Hwa, T. Identification of direct residue contacts in protein–protein interaction by message passing. *Proceedings of the National Academy of Sciences*, 106(1):67–72, 2009.

Xu, J. Distance-based protein folding powered by deep learning. *arXiv preprint arXiv:1811.03481*, 2018.

Zhou, J. and Troyanskaya, O. G. Deep supervised and convolutional generative stochastic network for protein secondary structure prediction. In *Proceedings of the 31th International Conference on Machine Learning, ICML 2014, Beijing, China, 21-26 June 2014*, pp. 745–753, 2014. URL http://jmlr.org/proceedings/papers/v32/zhou14.html.